Nonlinear Digital Filters, I. Pitas & A.N. Venetsanopoulos, Kluwer Academic, 1990.

CHAPTER 6

MORPHOLOGICAL IMAGE AND SIGNAL PROCESSING

6.1 THE PRINCIPLES OF MATHEMATICAL MORPHOLOGY

The final goal of image processing and analysis is, often, to segment the image into objects in order to analyze the geometric properties (e.g., the size) and the structure of the objects and recognize them. The analysis of the geometric objects must be quantitative, because only such an analysis and description of the geometric objects can provide a coherent mathematical framework for describing the spatial organization. The quantitative description of geometrical structures is the purpose of mathematical morphology [1].

Originally mathematical morphology was developed for the description of binary images and objects. An image object X is represented, in mathematical morphology terminology, as a set inside an n-dimensional Euclidean space $\mathbf{R}^n$. A binary image object X is represented by the set:

$$X = \{z: f(z)=1, \ z=(x,y) \in \mathbf{R}^2\} \tag{6.1.1}$$

The binary object background is the set X^c defined as follows:

$$X^c = \{z: f(z)=0, \ z=(x,y) \in \mathbf{R}^2\} \tag{6.1.2}$$

The function f is called the *characteristic function* of X. If the Euclidean grid $\mathbf{Z}^2$ is used instead of $\mathbf{R}^2$ for digitized binary images, definitions (6.1.1) and (6.1.2) become:

$$X = \{(i,j): f(i,j)=1, \ (i,j) \in \mathbf{Z}^2\} \tag{6.1.3}$$

$$X^c = \{(i,j): f(i,j)=0, \ (i,j) \in \mathbf{Z}^2\} \tag{6.1.4}$$

Later on, mathematical morphology was extended to describe and process multivalued (grayscale) images and objects. Multivalued images are functions $f(x,y)$ of the two spatial coordinates x,y, $(x,y) \in \mathbf{R}^2$:

$$(x,y) \in \mathbf{R}^2 \rightarrow f(x,y) \in \mathbf{R} \tag{6.1.5}$$

Grayscale images can be viewed as subsets of the Cartesian product $\mathbf{R}^2 \times \mathbf{R}$. If the multivalued image is defined over the Euclidean grid $\mathbf{Z}^2$, i.e., it is of the

form $f(i,j)$, $(i,j) \in \mathbf{Z}^2$, it can be represented as a subset of $\mathbf{Z}^2 \times \mathbf{R}$. Morphological transformations have applications not only in image analysis but also in image and signal filtering and processing. The so-called morphological filters [11] are a fruitful application of mathematical morphology in image and signal filtering. Also edge detectors based on morphological operators have been proposed [10]. A discussion of such applications can be found in subsequent sections.

An image object is described by a set in mathematical morphology, because its subparts can be described easier in this notation. The group of all the interrelationships among its subparticles gives the structure of the object, according to J. Serra [1]. According to this definition, an image object possesses no information, before an observer studies it. It is the observer, who sees from an image object only what he wants to look at [1]. Therefore, the object structure depends on the observer and it is not objective. The observer interacts with the object and transforms it to another, perhaps more expressive, object and measures certain properties of the new object. The tool of interaction is a simple object called a *structuring element* (e.g., a circle or a square). The mode of interaction is the *morphological transformation* $\psi(X)$ whose operation is described in Figure 6.1.1. Information about the object size, shape, connectivity, convexity, smoothness, and orientation can be obtained by transforming the original object with different structuring elements. Some psychological experiments [66] have revealed that human vision is active and that the mind has a structuring activity on even the simplest perceptive phenomena, i.e., for the mind to perceive an image it has to transform it [1]. Thus, there exists strong psychological motivation for the use of mathematical morphology in image processing and computer vision.

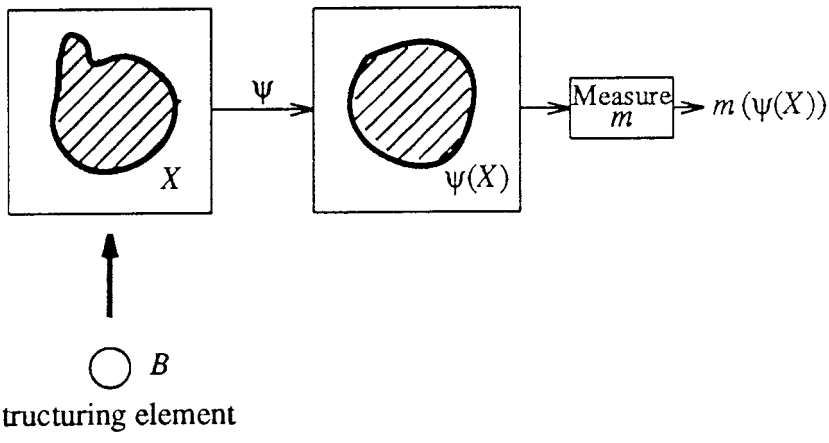

Figure 6.1.1: The methodology of mathematical morphology (adapted from [53]).

The performance of a morphological transformation depends on two factors: the structuring element and the transformation $\psi(X)$. There is a great variety of structuring elements. Their choice depends on the particular task, as will be seen later. The transformation function $\psi(X)$ must satisfy some constraints so that the morphological transformation is quantitative. These constraints form the *principles* of mathematical morphology [1, p.6]:

(1) **Translation invariance.** If X_z is the translate of the set $X \subset \mathbf{R}^2$ by a vector $z \in \mathbf{R}^2$, the translation invariance property can be stated as follows:

$$\psi(X_z) = [\psi(X)]_z \tag{6.1.6}$$

Translation invariance is a very natural requirement for any morphological operation, since the structure of the object does not generally change with its position in space.

(2) **Compatibility with change of scale.** If λ is a scaling factor, a morphological transformation $\psi(X)$ is compatible with change in scale, if a transformation $\psi_\lambda(X)$ can be constructed, such that:

$$\psi_\lambda(X) = \lambda\psi(\lambda^{-1}X) \tag{6.1.7}$$

Compatibility with magnification arises from the fact that, generally, the object structure does not change with scale.

(3) **Local knowledge.** Image objects are usually seen through windows (e.g., through an image frame). If for any bounded window M^* in which we want to know $\psi(X)$, we can find a bounded window M in which the knowledge of X is sufficient to perform the transformation locally (i.e., within M^*):

$$[\psi(X \cap M)] \cap M^* = \psi(X) \cap M^* \tag{6.1.8}$$

the transformation $\psi(X)$ requires only local knowledge of the image object X, and it is called *local*. Otherwise it is called *global*.

(4) **Semicontinuity.** The fourth principle of mathematical morphology describes the continuity properties of the morphological transformations. The definition of continuity is rather difficult and requires the description of some basic notions on limits. Let a_i, i=1,2,.. be a sequence of points of the topological space E. Let us suppose that there exists a point a such that we can find an arbitrary large index n so that $a_n \in N(a)$ for any neighborhood $N(a)$ of a. Such a point is called *adherent point* of this sequence. Let X_i, i=1,2,.. be a sequence of objects of the topologic space E. Let us also suppose that this sequence possesses adherent points. We denote by $\overline{\lim}\, X_n$ and by $\underline{\lim}\, X_n$ the union and the intersection of those adherent points, respectively. An example for the clarification of the notion of adherent points is given in Figure 6.1.2. Let X_n, ($n \geq 2$) denote the boundary of the rectangle shown in Figure 6.1.2. When n is even (n=2i), a slice of width w/i and height $h_i = h(1-1/i)/2$ is removed from

the top of the rectangle. When n is odd ($n=2i+1$), a slice of the same width and height is removed from the bottom of the rectangle. The union of all adherent points of X_n is the rectangle and the vertical line segment passing through its center. The intersection of the adherent points is the rectangle and its center. Having given those definitions, we can describe the fourth principle of mathematical morphology.

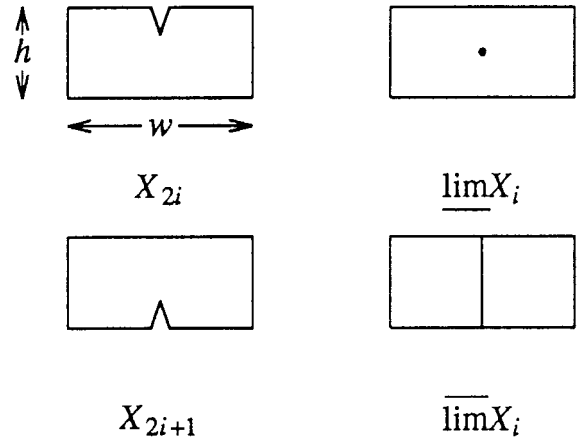

Figure 6.1.2: Example of adherent points (adapted from [1]).

Let X_n, $n=1,2,...$ be a sequence of closed objects tending toward a limit image object X. Let $\psi(X_n)$ be the sequence of the morphologically transformed objects. The morphological transformation is *semicontinuous*, if the sequence of transformed objects tends to $\psi(X)$. There are two types of semicontinuity: *upper* and *lower semicontinuity*. A morphological transformation $\psi(X)$ is upper semi-continuous if:

$$\overline{\lim}\, \psi(X_n) \subset \psi(X) \tag{6.1.9}$$

The upper semi-continuity property of a transformation is essentially a guarantee for the robustness of the transformation against small variations in the object structure. An example of a discontinuous transformation is shown in Figure 6.1.3. The transformation shown is the following:

$$\psi(X): \quad X \rightarrow \text{maximal inscribable disk in } X$$

Let us suppose that X is a rectangle and X_i is a decreasing sequence of objects, which tend to X. In this case, the limit $\psi(X_i)$ is different from $\psi(X)$. A similar discontinuity exists for increasing sequences X_i, as can also be seen in Figure 6.1.3.

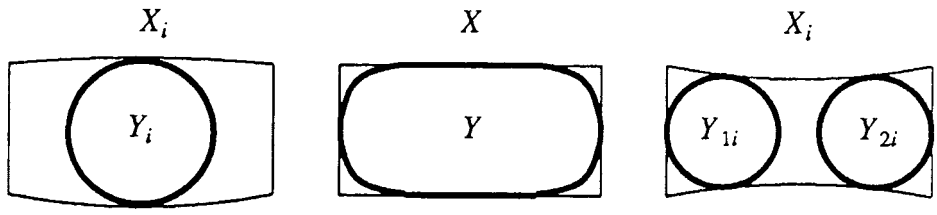

Figure 6.1.3: An example of discontinuous morphological transformation (adapted from [1]).

A much weaker notion is lower semicontinuity:

$$\underline{\lim}\,\psi(X_n) \supset \psi(X) \tag{6.1.10}$$

where $\underline{\lim} X_n$ is the intersection of all adherent points A. The principles (1)-(4) form a general framework for mathematical morphology. However, there exist several morphological operations (e.g., skeletonization) that do not conform with all above mentioned principles. Serra has dropped semicontinuity as a basic property of morphological transformations in [5]. Generally speaking, those principles can be followed as long as they do not pose problems in the development of morphological techniques.

All morphological transformations are non-reversible operations, except for some subclasses of the object X. In fact, the philosophy of mathematical morphology is not to restore the image but to *manage the loss of information* of an image through successive transformations [5]. The following properties are related to the ability of the morphological transformations to perform such a controlled loss of information.

(1) **Increasing.** $\psi(X)$ is increasing, when it preserves inclusion:

$$X \subset Y \Rightarrow \psi(X) \subset \psi(Y) \tag{6.1.11}$$

(2) **Anti-extensivity.** $\psi(X)$ is anti-extensive, if it shrinks X:

$$\psi(X) \subset X \tag{6.1.12}$$

(3) **Idempotence.** $\psi(X)$ is idempotent, when $\psi(X)$ is unchanged by the reapplication of the transformation:

$$\psi[\psi(X)] = \psi(X) \tag{6.1.13}$$

(4) **Homotopy.** Each object X is associated with an *homotopy tree.* Its root corresponds to the background X and its leaves to the components of X, as is seen in Figure 6.1.4. Homotopy is more severe than connectivity: a disk and a ring are both connected but not homotopic. A transformation is called

homotopic if it preserves the homotopy tree of X.

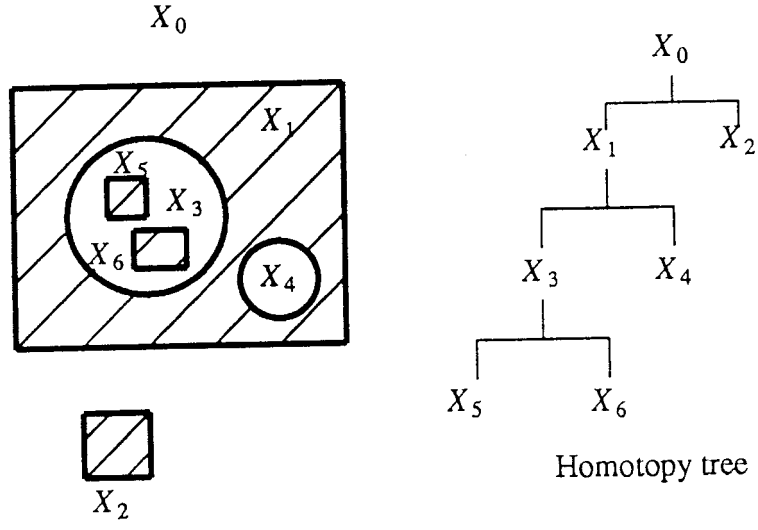

Figure 6.1.4: Homotopy tree.

These four properties are very important for the analysis of morphological transformations. However, other properties exist too, e.g., symmetrical treatment of the background, connectivity, and monotonicity.

Every morphological transformation ψ has its *dual* ψ^*. The transformation $\psi(X)$ transforms also the image object background X^c to $\psi(X^c)$. This operation is the dual $\psi^*(X)$ with respect to complementation:

$$\psi^*(X) = [\psi(X^c)]^c \tag{6.1.14}$$

Several dual morphological transformations will be discussed in the subsequent sections. Duality applies also to the properties of the morphological transformations. The dual properties of anti-extensivity, idempotence, and homotopy are extensivity, idempotence, and homotopy [1, p.588]. It is important to note that the dual of the increasing property is the same property. If $\psi(X)$ is increasing, then $\psi^*(X)$ is increasing also.

Before we proceed to the definition of morphological transformations it is important to review some notions of set theory. Let E be an arbitrary set and $p(E)$ be its *power set*, i.e., the set of all subsets of E:

$$p(E) = \{X : X \subset E\} \tag{6.1.15}$$

Throughout this chapter, E will denote either the Euclidean space $\mathbf{R}^n$, or its digital counterpart $\mathbf{Z}^n$. The set $p(E)$ is a *Boolean algebra* and has the following

properties [2]:

(1) $p(E)$ is a *complete lattice*, i.e., it is provided with a partial ordering relation called *inclusion* and denoted by $\subset$. Every family of sets $X_i \in p(E)$ has a least upper bound, namely the union $\cup X_i$, and a greatest lower bound, namely the intersection $\cap X_i$, which both belong to $p(E)$.

(2) The lattice $p(E)$ is *distributive:*

$$X \cup (Y \cap Z) = (X \cup Y) \cap (X \cup Z), \qquad \forall X,Y,Z \in p(E) \tag{6.1.16}$$

(3) The lattice $p(E)$ is *complemented*, i.e., for each set X exists its *complement* X^c:

$$X \cup X^c = E \qquad X \cap X^c = \varnothing \tag{6.1.17}$$

The set difference in $p(E)$ is defined as follows:

$$X - Y = X \cap Y^c \tag{6.1.18}$$

i.e., $X-Y$ is the part of X that does not belong to Y. For two given sets $B,X \in p(E)$, we may have:

(a) B is included in X: $B \subset X$ meaning $B \cap X = B$

(b) B *hits* X: $B \uparrow X$ meaning $B \cap X \neq \varnothing$

(c) B *misses* X: $B \subset X^c$ meaning $B \cap X = \varnothing$.

These definitions are illustrated in Figure 6.1.5. Although they are rather abstract, they will be useful in the subsequent sections.

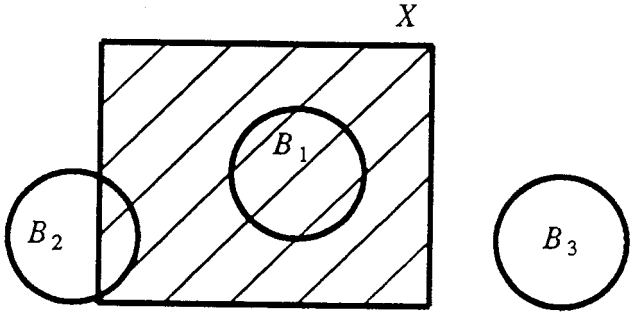

Figure 6.1.5: Set B_1, B_2, B_3 is included, hits, and misses object X respectively.

Another notion which is useful in mathematical morphology is the notion of the topologically open and closed set, which is defined as follows [1, p. 66]. A topological space is a pair consisting of a set E and a collection of subsets of

E called open sets, satisfying the three following properties:

(1) Every union of open sets is open.

(2) Every *finite* intersection of open sets is open.

(3) The set E and the empty set $\varnothing$ are open.

A subset X of E is closed if X^c is open.

If $E=\mathbf{R}$, then the open sets are the open intervals of the form $Y=(a,b)$. If Y_i, $i=1,...,n$ are open sets in $\mathbf{R}$, the set $Y_1 \times Y_2 \times \cdots \times Y_n$ is an *open interval* in $\mathbf{R}^n$. Every union of open intervals in $\mathbf{R}^n$ is an open set. There are sets that are both open and closed. Such sets are the subsets of $\mathbf{Z}^n$.
Finally, the De Morgan's laws will be stated:

$$(X \cup Y)^c = X^c \cap Y^c \tag{6.1.19}$$

$$(X \cap Y)^c = X^c \cup Y^c \tag{6.1.20}$$

Having defined all basic mathematical notions, we proceed to the definitions of the basic morphological transformations.

6.2 EROSION AND DILATION IN THE EUCLIDEAN SPACE

The analysis of the elementary morphological transformations is restricted in the Euclidean space, i.e., $E=\mathbf{R}^n$ or $\mathbf{Z}^n$, because this space is important for image processing applications. In this section we shall work only with binary images. The binary objects X are of the form (6.1.1) or (6.1.3) and E is either $\mathbf{R}^2$ or $\mathbf{Z}^2$. In the second case, the binary image object X can be viewed as a set of integer pairs (i,j). Each pair gives the coordinates of an image pixel, with respect to two basis unit vectors. The length of the unit vectors is equal to the sampling period along each direction. If the angle between the basis vector is 60°, the Euclidean grid is the hexagonal one. If the angle is 90°, the Euclidean grid is the rectangular one, which is used in the vast majority of image processing applications.

The simplest morphological transformation is *erosion* and *dilation* [1]. These two operations are based on *Minkowski set addition and subtraction* [1,7]. Let us suppose that a, b are two vectors, which are members of the sets $A,B \in E$ respectively. If z is the result of the vector addition of a and b, the Minkowski addition of A,B is given by:

$$A \oplus B = \{z \in E: \quad z=a+b, \ a \in A, \ b \in B\} \tag{6.2.1}$$

If A_b is the translate of the set A by the vector b:

$$A_b = \{z \in E: \ z=a+b, \ a \in A\} \tag{6.2.2}$$

the Minkowski addition is also given by:

$$A \oplus B = \bigcup_{b \in B} A_b \tag{6.2.3}$$

The equivalence of (6.2.1) and (6.2.3) is easily proven:

$$\begin{aligned} A \oplus B &= \bigcup_{b \in B} A_b = \bigcup_{b \in B} \{z \in E: \quad z=a+b, a \in A\} \\ &= \{z \in E: z=a+b, a \in A, b \in B\} \end{aligned} \tag{6.2.4}$$

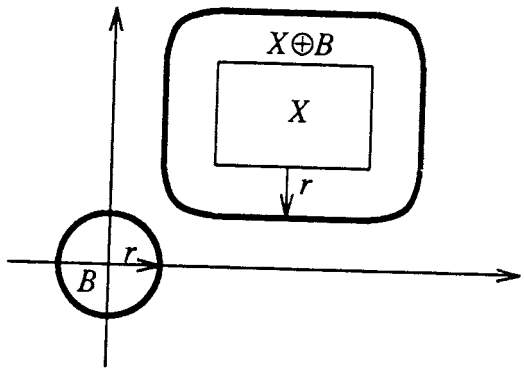

Figure 6.2.1: Minkowski addition of a rectangle and a disk.

The Minkowski set subtraction of B from A, denoted by $A \ominus B$, is defined by:

$$A \ominus B = \bigcap_{b \in B} A_b \tag{6.2.5}$$

Minkowski subtraction is the dual operation of Minkowski addition:

$$\begin{aligned} A \oplus B &= (A^c \ominus B)^c \\ A \ominus B &= (A^c \oplus B)^c \end{aligned} \tag{6.2.6}$$

Proof: Let $z \in (A^c \ominus B)^c$. Then $z \notin A^c \ominus B$. This happens if and only if there exists a $b \in B$ such that $z \notin A_b^c$. This also happens if and only if there exists a $b \in B$ such that $z \in A_b$, i.e. $z \in A \oplus B$.
The notions of Minkowski addition and subtraction are clarified in Figures 6.2.1 and 6.2.2.

Let us suppose that there exists an image object X and a structuring element B. The set B^s is called symmetric of B with respect to the origin if:

$$B^s = \{-b: \quad b \in B\}$$

Therefore, B^s is obtained by rotating B 180 degrees in the plane as is seen in

Figure 6.2.3. If B is symmetric about the origin, there is no difference between B and B^s. Some symmetric structuring elements are shown in Figure 6.2.4.

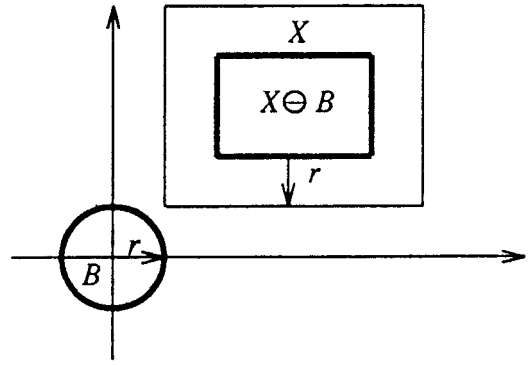

Figure 6.2.2: Minkowski subtraction of a disk from a rectangle .

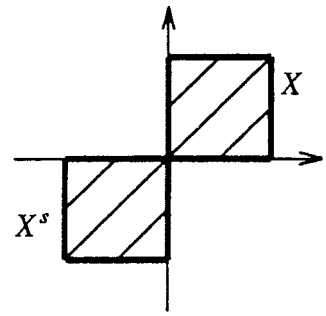

Figure 6.2.3: Definition of the symmetric set X^s of the set X about the origin.

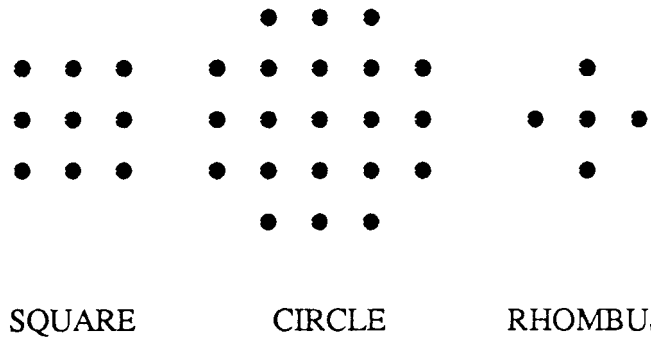

Figure 6.2.4: Symmetric structuring elements.

The *dilation* of X by B is the Minkowski set addition of X with B^s:

$$X \oplus B^s = \bigcup_{b \in B} X_{-b} \tag{6.2.7}$$

Another definition of dilation is the following:

$$X \oplus B^s = \{z \in E : B_z \cap X \neq \emptyset\} = \{z : B_z \uparrow X\} \tag{6.2.8}$$

Proof: The equivalence of (6.2.7) and (6.2.8) is proven as follows:

$$\{z \in E : B_z \cap X \neq \emptyset\} = \{z \in E : \text{exists } a \in X \text{ such that } a \in B_z\} =$$

$$\{z \in E : \text{exists } a \in X \text{ such that } a - z \in B\} =$$

$$\{z \in E : \text{exists } a \in X,\ b \in B \text{ such that } z = a - b\} =$$

$$\{z \in E : \text{exists } a \in X,\ b' \in B^s \text{ such that } z = a + b'\} = X \oplus B^s \tag{6.2.9}$$

Definition (6.2.8) suggest that the dilation $X \oplus B^s$ includes all the translates B_z of B which have common points with X. Therefore, dilation is an expanding operator, as it is seen in Figure 6.2.5.

The *erosion* of X by B is the Minkowski set subtraction of B^s from X:

$$X \ominus B^s = \bigcap_{b \in B} X_{-b} \tag{6.2.10}$$

A fully equivalent definition of erosion is the following:

$$X \ominus B^s = \{z \in E : B_z \subset X\} \tag{6.2.11}$$

Proof:

$$\{z \in E : B_z \subset X\} = \bigcap_{b \in B} \{z : b + z \in X\} = \bigcap_{b \in B} X_{-b} = X \ominus B^s \tag{6.2.12}$$

Definition (6.2.11) shows that erosion $X \ominus B^s$ includes all the translates B_z which are included in X. Therefore, it is a shrinking operator. An example of erosion is shown in Figure 6.2.5.

The definitions of dilation and erosion used are the same as those given by Serra [1,5]. Other authors, e.g., Haralick et al. [4], Giardina et al. [8,9], give slightly different definitions and they make no distinction between dilation and Minkowski set addition. The differences between dilation, Minkowski addition and erosion, Minkowski subtraction, according to definitions (6.2.7), (6.2.10), are illustrated in Figure 6.2.6.

(a)

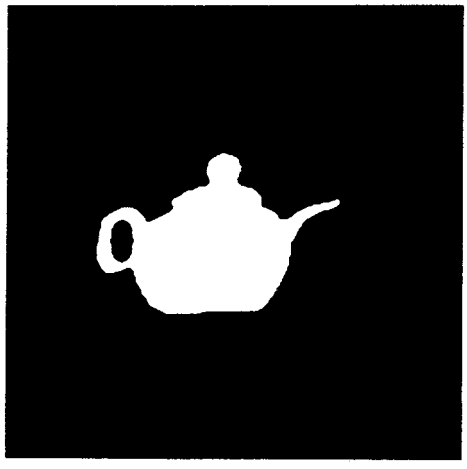

(b)

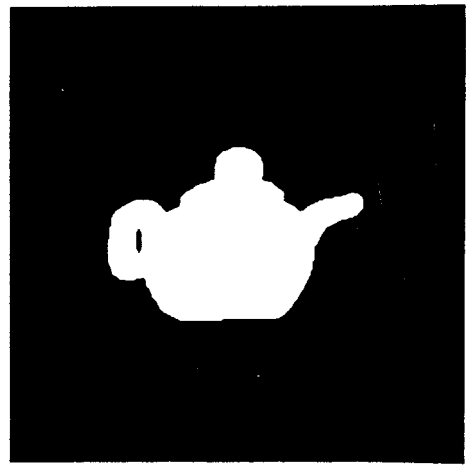

(c)

(d)

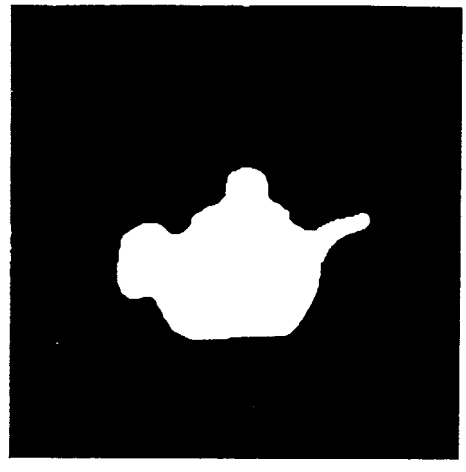

(e)

Figure 6.2.5: (a) Image object POT; (b) Erosion of POT by the CIRCLE

structuring element; (c) Dilation of POT by the CIRCLE structuring element; (d) Opening of POT by the structuring element *CIRCLE⊕CIRCLE*; (e) Closing of POT by the structuring element *CIRCLE⊕CIRCLE*.

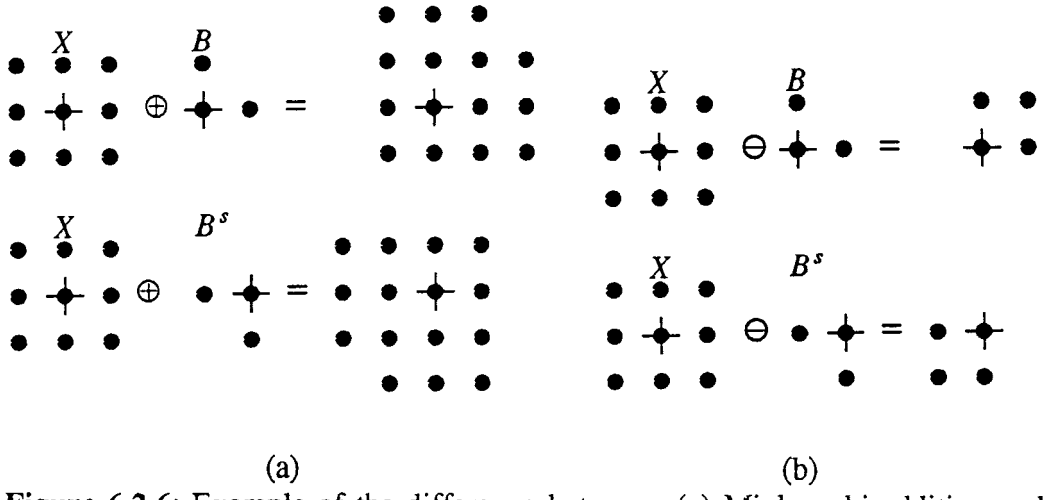

(a) (b)

Figure 6.2.6: Example of the difference between: (a) Minkowski addition and dilation, (b) Minkowski subtraction and erosion.

Minkowski set addition and subtraction, erosion and dilation possess several interesting properties. They are:

(1) Commutative

$$A \oplus B = B \oplus A \tag{6.2.13}$$

(2) Associative

$$A \oplus (B \oplus C) = (A \oplus B) \oplus C \tag{6.2.14}$$

The proofs of (6.2.13-14) are very simple and they are omitted.

(3) Translation invariance of Minkowski addition and dilation

$$A_z \oplus B = (A \oplus B)_z \tag{6.2.15}$$

Proof: Every element $y \in A_z \oplus B$ has the form $y=(a+z)+b$, $a \in A$, $b \in B$. Therefore, $y=(a+b)+z$ and it is also an element of $(A \oplus B)_z$.

Corollaries

$$A \oplus B_1 \oplus B_2 \oplus \cdots \oplus (B_n)_z \oplus \cdots \oplus B_N = (A \oplus B_1 \oplus \cdots \oplus B_N)_z \tag{6.2.16}$$

$$A_z \oplus B_{-z} = A \oplus B \tag{6.2.17}$$

(4) Increasing property

$$A \subseteq B \Rightarrow A \oplus D \subseteq B \oplus D \tag{6.2.18}$$

Proof: Let $x \in A \oplus D$. Thus $x=a+d$, for $a \in A$, $d \in D$. Since $A \subset B$, it implies $a \in B$. Therefore, $x \in B \oplus D$ and (6.2.18) is valid.
According to (6.2.18) dilation is an increasing transformation.

(5) Distributive properties of Minkowski addition and dilation

$$(A \cup B) \oplus C = (A \oplus C) \cup (B \oplus C) \tag{6.2.19}$$

$$A \oplus (B \cup C) = (A \oplus B) \cup (A \oplus C) \tag{6.2.20}$$

Proof:

$$(A \cup B) \oplus C = \bigcup_{x \in A \cup B} C_x = \left(\bigcup_{x \in A} C_x\right)\left(\bigcup_{x \in B} C_x\right) = (A \oplus C) \cup (B \oplus C) \tag{6.2.21}$$

(6.2.20) follows from (6.2.19) from the commutativity of Minkowski addition.
(6.2.19) suggests that dilation possesses the distributivity with set union. (6.2.20) is more important since it suggests that, if a structuring element B can be decomposed in a union of structuring elements, the image can be dilated independently by the two structuring elements and that the results can be combined by set union.
However, Minkowski addition is not distributive with set intersection:

$$(A \cap B) \oplus C \subseteq (A \oplus C) \cap (B \oplus C) \tag{6.2.22}$$

$$A \oplus (B \cap C) \subseteq (A \oplus B) \cap (A \oplus C) \tag{6.2.23}$$

Proof: If $x \in (A \cap B) \oplus C$, it is given by $x=y+c$, $y \in (A \cap B)$, $c \in C$. The fact $y \in (A \cap B)$ implies that $y \in A$ and $y \in B$. Therefore, x belongs to $A \oplus C$ and to $B \oplus C$. Hence it belongs to $(A \oplus C) \cap (B \oplus C)$. Thus (6.2.22) is valid. (6.2.23) comes from (6.2.22) by using the commutativity of Minkowski addition.

(6) Translation invariance of Minkowski subtraction and erosion

$$A_z \ominus B = (A \ominus B)_z \tag{6.2.24}$$

$$A \ominus B_z = (A \ominus B)_z \tag{6.2.25}$$

Proof:

$$A_z \ominus B = ((A_z)^c \oplus B)^c = ((A^c)_z \oplus B)^c = [(A^c \oplus B)^c]_z = (A \ominus B)_z \tag{6.2.26}$$

$$A \ominus B_z = (A^c \oplus B_z)^c = (A^c \oplus B)_z^c = (A \ominus B)_z \tag{6.2.27}$$

The duality property (6.2.6) and the translation invariance of Minkowski addition have been used in (6.2.26-27). (6.2.24-25) suggest that erosion is translation invariant.

(7) Increasing property of Minkowski subtraction and erosion

$$A \subseteq B \Rightarrow A \ominus D \subseteq B \ominus D \tag{6.2.28}$$

Proof:

$$A \ominus D = \bigcap_{d \in D} A_d \subseteq \bigcap_{d \in D} B_d = B \ominus D \tag{6.2.29}$$

It should be mentioned that both erosion and dilation are increasing transformations, although they are dual operations.

(8) Distributivity properties of Minkowski subtraction and erosion

$$A \ominus (B \cup C) = (A \ominus B) \cap (A \ominus C) \tag{6.2.30}$$

$$(B \cap C) \ominus A = (B \ominus A) \cap (C \ominus A) \tag{6.2.31}$$

Proof: By applying DeMorgan's law and duality, it is found that:

$$\begin{aligned} A \ominus (B \cup C) &= [A^c \oplus (B \cup C)]^c = [(A^c \oplus B) \cup (A^c \oplus C)]^c \\ &= (A^c \oplus B)^c \cap (A^c \oplus C)^c = (A \ominus B) \cap (A \ominus C) \end{aligned} \tag{6.2.32}$$

By applying DeMorgan's law and duality, we find:

$$\begin{aligned} (B \cap C) \ominus A &= [(B \cap C)^c \oplus A]^c = [(B^c \cup C^c) \oplus A]^c = [(B^c \oplus A) \cup (C^c \oplus A)]^c \\ &= (B^c \oplus A)^c \cap (C^c \oplus A)^c = (B \ominus A) \cap (C \ominus A) \end{aligned} \tag{6.2.33}$$

Property (6.2.31) asserts a right distributivity of Minkowski subtraction over intersection. However, left distributivity does not hold:

$$A \ominus (B \cap C) \supseteq (A \ominus B) \cup (A \ominus C) \tag{6.2.34}$$

Proof: By using DeMorgan's law and property (6.2.23), we find

$$\begin{aligned} A \ominus (B \cap C) &= [A^c \oplus (B \cap C)]^c \supseteq [(A^c \oplus B) \cap (A^c \oplus C)]^c \\ &= (A \ominus B) \cup (A \ominus C) \end{aligned} \tag{6.2.35}$$

(9) Distributivity between Minkowsky addition and subtraction

$$A \ominus (B \oplus C) = (A \ominus B) \ominus C \tag{6.2.36}$$

Proof:

$$A \ominus (B \oplus C) = [A^c \oplus (B \oplus C)]^c = [(A^c \oplus B) \oplus C]^c$$
$$= (A^c \oplus B)^c \ominus C = (A \ominus B) \ominus C \tag{6.2.37}$$

The property (6.2.36) is very important for the practical implementation of the erosion. If a structuring element B^s can be decomposed as the dilation of K structuring elements

$$B^s = B_1^s \oplus B_2^s \oplus \cdots \oplus B_K^s \tag{6.2.38}$$

the erosion $X \ominus B^s$ can be implemented in K steps as follows:

$$X \ominus B^s = (\ldots((X \ominus B_1^s) \ominus B_2^s) \cdots \ominus B_K^s) \tag{6.2.39}$$

The same decomposition can be used for the implementation of the dilation $X \oplus B^s$, by virtue of (6.2.14):

$$X \oplus B^s = (\cdots((X \oplus B_1^s) \oplus B_2^s) \oplus \cdots \oplus B_K^s) \tag{6.2.40}$$

Both decompositions (6.2.39-40) will be used in subsequent sections. A structuring element decomposition of the form (6.2.38) is shown in Figure 6.2.7. The theory for optimal structuring element decomposition is presented in [59].

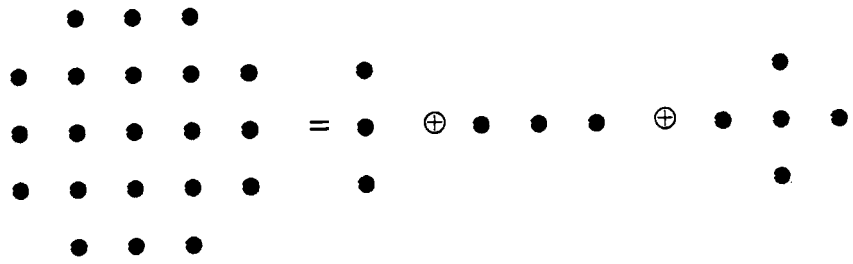

Figure 6.2.7: Decomposition of the structuring set CIRCLE in the Minkowski addition of smaller structuring elements.

(6.2.36) assures the left distributivity of erosion with dilation. The opposite is not true:

$$A \oplus (B \ominus C) \subseteq (A \oplus B) \ominus C \tag{6.2.41}$$

Proof: By using the translation invariance (6.2.15) and the inequality (6.2.23) it is found that

$$A\oplus(B\ominus C)=A\oplus(\underset{z\in C}{\cap}B_z)\subseteq\underset{z\in C}{\cap}(A\oplus B_z)=\underset{z\in C}{\cap}(A\oplus B)_z=(A\oplus B)\ominus C \quad (6.2.42)$$

Erosions and dilations are special cases of the *hit-or-miss transformation*. Let X be an image object and A, B two structuring elements. The hit-or-miss transformation $X\circledast(A,B)$ is defined as [1, pp. 39,270],[5]:

$$X\circledast(A,B)=(X\ominus A^s)-(X\oplus B^s)=(X\ominus A^s)\cap(X^c\ominus B^s) \quad (6.2.43)$$

The general hit-or-miss transformation is the logical ancestor of all other transformations involved in mathematical morphology. For example, if $B=\varnothing$, $X\circledast(A,B)$ equals to the erosion $X\ominus A^s$. However, it is neither increasing, nor extensive, nor anti-extensive and, therefore, it has limited applications.

6.3 CLOSINGS AND OPENINGS

Erosion is generally a non-reversible operation. Therefore, an erosion followed by a dilation does not generally recover the original object X. Instead it defines a new morphological transformation called *opening* X_B:

$$X_B=(X\ominus B^s)\oplus B \quad (6.3.1)$$

Its dual operation is the *closing* X^B:

$$X^B=(X\oplus B^s)\ominus B \quad (6.3.2)$$

The duality between opening and closing is expressed by the following relations:

$$(X^B)^c=(X^c)_B \quad (6.3.3)$$

$$(X_B)^c=(X^c)^B \quad (6.3.4)$$

Proof:

$$(X^B)^c=[(X\oplus B^s)\ominus B]^c=(X\oplus B^s)^c\oplus B=(X^c\ominus B^s)\oplus B=(X^c)_B$$

$$(X_B)^c=[(X\ominus B^s)\oplus B]^c=(X\ominus B^s)^c\ominus B=(X^c\oplus B^s)\ominus B=(X^c)^B$$

The opening X_B consists of the union of those translates of B that lie inside X:

$$X_B=\cup\{B_z:\ B_z\subset X\} \quad (6.3.5)$$

Proof: The opening X_B is given by $X_B=\underset{z\in(X\ominus B^s)}{\cup}B_z$. We have to prove that $B_z\subseteq X$, when $z\in(X\ominus B^s)$. Each element b' of B_z has the form $b'=b+z$. For

each member $z \in (X \ominus B^s)$ an element X can be found such that $z=x-b$. Therefore, each element of B_z satisfies $b'=b+z=x \in X$. Thus $B_z \subset X$ and

$$X_B = \bigcup_{z \in (X \ominus B^s)} B_z = \cup\{B_z : B_z \subset X\}$$

(6.3.5) is an important property because it shows that the opening smooths the contours of X, cuts the narrow isthmuses, suppresses the small islands and the sharp capes of X. This behavior can be seen in Figure 6.2.5.
By duality the closing X^B consists of the intersection of the complements of the translates of B that lie outside X:

$$X^B = \cap\{(B_z)^c : B_z \subset X^c\} \tag{6.3.6}$$

Proof: By using the duality property:

$$X^B = [(X^B)^c]^c = [(X^c)_B]^c = [\cup\{B_z : B_z \subset X^c\}]^c = \cap\{(B_z)^c : B_z \subset X^c\}$$

By duality, closing blocks up narrow channels, small holes and thin gulfs of X, as is seen in Figure 6.2.5.
The opening is an antiextensive, idempotent, and increasing transformation:

$$(1)\quad X_B \subset X \quad \text{(antiextensive)} \tag{6.3.7}$$

$$(2)\quad X_1 \subset X_2 \Rightarrow (X_1)_B \subset (X_2)_B \quad \text{(increasing)} \tag{6.3.8}$$

$$(3)\quad (X_B)_B = X_B \quad \text{(idempotent)} \tag{6.3.9}$$

Proof:

(1) $X_B = \cup\{B_z : B_z \subset X\} \subset X$

(2) $(X_1)_B = \cup\{B_z : B_z \subset X_1\} \subset \cup\{B_z : B_z \subset X_2\} = (X_2)_B$

(3) $(X_B)_B = [[(X \ominus B^s) \oplus B] \ominus B^s] \oplus B = (X \ominus B^s)^{B'} \oplus B \supset (X \ominus B^s) \oplus B = X_B$

The containment comes from the fact $X^B \supset X$ (see (6.3.10)). On the other hand, by using (6.3.7) $(X_B)_B \subset X_B$. Therefore, (6.3.9) is valid.
Similar properties are valid for closing due to duality:

$$(1)\quad X^B \supset X \quad \text{(extensive)} \tag{6.3.10}$$

$$(2)\quad X_1 \subset X_2 \Rightarrow (X_1)^B \subset (X_2)^B \quad \text{(increasing)} \tag{6.3.11}$$

$$(3)\quad (X^B)^B = X^B \quad \text{(idempotent)} \tag{6.3.12}$$

Proof:

(1) $(X^B)^c = (X^c)_B \subset X^c$. Therefore, $X^B \supset X$.

(2) $[(X_1)^B]^c = (X_1^c)_B \supset (X_2^c)_B = [(X_2)^B]^c$. Therefore, $(X_1)^B \subset (X_2)^B$.

(3) $(X^B)^B = \{[(X^B)^B]^c\}^c = \{[(X^B)^c]_B\}^c = \{[(X^c)_B]_B\}^c = \{(X^c)_B\}^c = X^B$.

The extensive, increasing, and idempotent properties of opening and closing are

very simple but powerful and important for theoretical and practical reasons.

In many cases it is important to know which objects X are invariant to opening with B. Such objects are said to be *open with respect to* B. The objects that are invariant to closing with B are called *closed with respect to* B. The following property is valid due to duality:

$$X_B = X \Rightarrow (X^c)^B = X^c \tag{6.3.13}$$

$$X^B = X \Rightarrow (X^c)_B = X^c \tag{6.3.14}$$

i.e., if X is open with respect to B, X^c is closed with respect to B.

Proof: By duality

$$(X^c)^B = (X_B)^c = X^c$$

$$(X^c)_B = (X^B)^c = X^c$$

The following two propositions define the structure of the open and closed sets X with respect to a structuring element B.

Proposition 1: X is B-open, if and only if there exists a set A such that $X=A \oplus B$.

Proof: (Necessity) If X is B-open, then $X=(X \ominus B^s) \oplus B$ and A is given by $A=X \ominus B^s$.
(Sufficiency) Let us suppose that $X=A \oplus B$. Its opening is given by

$$X_B = (X \ominus B^s) \oplus B = [(A \oplus B) \ominus B^s] \oplus B = A^{B^s} \oplus B \supset A \oplus B = X$$

On the other hand, by antiextensivity $X_B \subset X$. Therefore, $X_B=X$.

Proposition 2: X is B-closed, if and only if there exists a set A such that $X=A \ominus B$.
Proof: (Necessity) If X is B-closed, then $X=(X \oplus B^s) \ominus B$ and A is given by $A=X \oplus B^s$.
(Sufficiency) Let us suppose that $X=A \ominus B$. Then $X^c=A^c \oplus B$ and it is B-open according to proposition 1. Therefore, X is B-closed according to (6.3.14).

The idempotence of opening can be generalized as follows. If A is B-open, then:

$$(X_B)_A = X_A \tag{6.3.15}$$

$$(X_A)_B = X_A \tag{6.3.16}$$

Similarly the idempotence of closing can be generalized. If A^c is B-closed then:

$$(X^B)^A = X^A \tag{6.3.17}$$

$$(X^A)^B = X^A \tag{6.3.18}$$

Furthermore, if A is B-open the following inclusion properties hold:

$$X_A \subset X_B \subset X \subset X^B \subset X^A \tag{6.3.19}$$

The proof of the properties (6.3.15-19) can be found in [9, p.111].

Until now only the morphological transformations of binary images have been considered. The analysis of gray-level morphological transformations is considered in the next section.

6.4 GRAYSCALE MORPHOLOGY

The notions and morphological transformations of a binary image can also be extended to grayscale images. Such images can be viewed as three-dimensional surfaces that usually have very interesting and nice landscapes. These surfaces can be modified by sliding structuring elements, leading to a variety of morphological transformations. Historically, the literature on the morphology of (graytone) functions starts from the second half of the seventies. J. Serra (1975) extended the hit-or-miss transformation and the size distributions to functions. Lantuejoul (1977) described the functions by their watersheds. Sternberg (1979) introduced the notion of umbra and several related transformations. Meyer (1977) developed contrast descriptors based on the top-hat transformation. Goetcherian contributed to the notion of lower skeleton (1979) and to the connection of mathematical morphology with fuzzy logic (1980). Rosenfeld (1977) proposed a generalization of connectivity functions. Recently Preston (1983) introduced the Ξ Filters, Lantuejoul and Serra (1982) introduced the morphological filters, and Maragos (1985) and Stevenson et al. (1987) have studied their connection to order statistic filters and their applications in image coding.

The bridge to use mathematical morphology for grayscale functions is the creation of a link between functions and sets. Such links are important because an image is a two-dimensional function $f(x,y)$, $(x,y) \in \mathbf{R}^2$ or $\mathbf{Z}^2$. Therefore, an effort will be made to describe an image by sets, and then to apply the known morphological transformations on those sets.

6.5 LINKS BETWEEN FUNCTIONS AND SETS

One of the most important links between sets and functions is the notion of *umbra*, introduced by Sternberg [17,18] and shown in Figure 6.5.1. If a function $f(x)$ has domain $D \subset \mathbf{R}^n$ or $D \subset \mathbf{Z}^n$ and takes values in $\mathbf{R}$:

$$x \in D \rightarrow f(x) \in \mathbf{R} \tag{6.5.1}$$

its umbra $U(f)$ is a subset of the Cartesian product $D \times \mathbf{R}$ consisting of those points of $D \times \mathbf{R}$, which occupy the space below the graph of $f(x)$ and down to $-\infty$:

$$U(f) = \{(x,y) \in D \times \mathbf{R}: f(x) \geq y\} \tag{6.5.2}$$

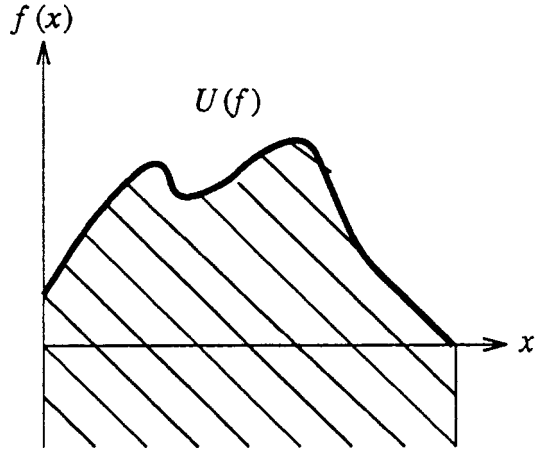

Figure 6.5.1: Definition of the umbra of a function.

In usual images the region of support D is a subset of $\mathbf{R}^2$. Therefore, their umbra is a subset of $\mathbf{R}^2 \times \mathbf{R} = \mathbf{R}^3$. A unique umbra $U(f)$ corresponds to any real-valued upper semicontinuous (u.s.c.) function $f(x)$. The function $f(x)$ can be reconstructed from its umbra as follows:

$$f(x) = \max\{y \in \mathbf{R}: (x,y) \in U(f)\} \tag{6.5.3}$$

(6.5.3) would be more mathematically concise if *supremum* (*sup*) were used instead of max, because y is a continuous variable and $y \in \mathbf{R}$. However, we use the max operator throughout, because in all practical cases y is discretized. The careful reader should substitute *sup* to *max* in appropriate circumstances. A concept related to umbra is the *top surface* $T(X)$ of a set $X \subset D \times \mathbf{R}$:

$$T[X](x) = \max\{y \in \mathbf{R}: (x,y) \in X\} \tag{6.5.4}$$

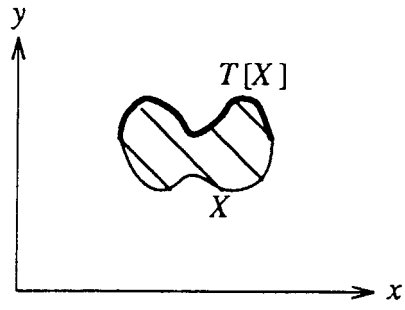

Figure 6.5.2: Definition of the top surface of a set.

which is illustrated in Figure 6.5.2. By combining (6.5.4) and (6.5.3), it is found that:

$$T[U(f)](x) = f(x) \tag{6.5.5}$$

Therefore, the top surface and the umbra inverse each other. In the following some properties of the umbra are given.

Proposition 1: Let $X \subseteq D \times \mathbf{R}$. Then $X \subseteq U[T(X)]$.

Proposition 2: If A is an umbra, then $A = U[T(A)]$.

Let us define the following ordering of functions:

$$f \leq g \longleftrightarrow f(x) \leq g(x) \quad \forall x \in D$$

Then the following property is valid:

Proposition 3: If $f \leq g$, then $U(f) \subseteq U(g)$.
Two new pointwise operations can be defined between two functions f, g:

$$(f \wedge g)(x) = \min(f(x), g(x)), \quad \forall x \in D \tag{6.5.6}$$

$$(f \vee g)(x) = \max(f(x), g(x)), \quad \forall x \in D \tag{6.5.7}$$

Their umbrae possess the following form:

Proposition 4:

$$U(f \wedge g) = U(f) \cap U(g) \tag{6.5.8}$$

$$U(f \vee g) = U(f) \cup U(g) \tag{6.5.9}$$

as can be seen in Figure 6.5.3.

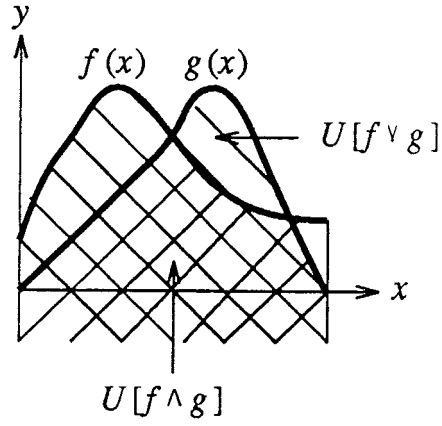

Figure 6.5.3: Umbrae of the maximum and the minimum of two functions.

Proposition 5: Suppose that A,B are umbrae. Then $A \oplus B, A \ominus B$ are umbrae.

Finally, a proposition similar to proposition 3 is valid for the top of surface:

Proposition 6: If $A \subseteq B$, then $T[A](x) \leq T[B](x)$.

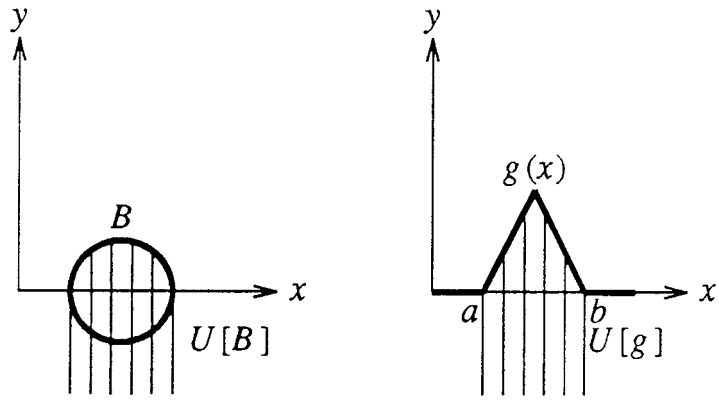

Figure 6.5.4: Examples of the umbra of a structuring element and of a structuring function.

The notion of umbra can easily be extended to the umbra of a set and of a structuring element, as is seen in Figure 6.5.4. In the next section, the importance of umbra in the definition of morphological transformations will be shown. Before doing this, another important link between functions and sets will be presented.

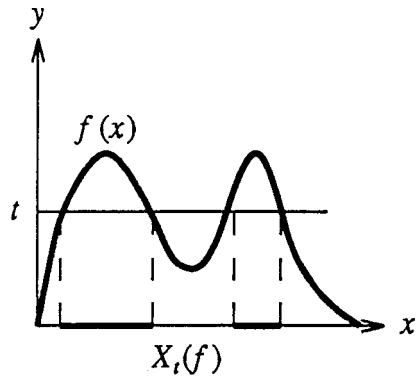

Figure 6.5.5: Definition of the cross-section of a function.

The *cross-section* of a function $f(x)$ at level t is given by:

$$X_t(f) = \{x \in D : f(x) \geq t\}, \quad -\infty < t < \infty \tag{6.5.10}$$

and is presented in Figure 6.5.5. It greatly resembles the *threshold decomposition* of ranked-order filters discussed in chapter 5. Obviously, $X_t(f) \subseteq D$. Cross-sections $X_t(f)$ are sets. Therefore, a function f can be decomposed to the sets $X_t(f)$, $-\infty < t < \infty$. Given the function cross-sections, the function itself can be reconstructed as follows:

$$f(x) = \max\{t \in \mathbf{R}: x \in X_t\} \tag{6.5.11}$$

The function cross-sections possess similar properties with umbra.

In a previous section some general properties of the morphological transformations have been given, namely the translation-invariant, increasing, extensive, and idempotent properties. Their generalization to the grayscale morphological operations is simple. Having defined all important links between sets and functions, we are ready for the transition to grayscale morphological transformations.

6.6 GRAYSCALE MORPHOLOGICAL TRANSFORMATIONS

Let us denote by $g(x)$ a simple function called *structuring function*. The simplest form of such a function is of the form:

$$g(x) = 0, \qquad x \in G \tag{6.6.1}$$

where G is its domain, which is a subset of $\mathbf{R}^n$. The umbra of a function having $G=[a,b] \subset \mathbf{R}$ is shown in Figure 6.5.4. Functions of the form (6.6.1) are equivalent to structuring sets. The symmetric function $g^s(x)$ with respect to the origin is given by

$$g^s(x) = g(-x) \tag{6.6.2}$$

If D is the domain of f and G is the domain of the structuring function g, the Minkowski addition of a function $f(x)$ by $g(x)$, denoted by $f \oplus g$ is defined by:

$$[f \oplus g](x) = \max_{\substack{z \in D \\ z-x \in G}} \{f(z)+g(x-z)\} \tag{6.6.3}$$

The Minkowski subtraction of $f(x)$ by $g(x)$ is defined by:

$$[f \ominus g](x) = \min_{\substack{z \in D \\ z-x \in G}} \{f(z)-g(x-z)\} \tag{6.6.4}$$

The grayscale dilation $f \oplus g^s$ and erosion $f \ominus g^s$ are given by:

$$[f \oplus g^s](x) = \max_{\substack{z \in D \\ z-x \in G}} \{f(z)+g(z-x)\} \tag{6.6.5}$$

$$[f \ominus g^s](x) = \min_{\substack{z \in D \\ z-x \in G}} \{f(z)-g(z-x)\} \tag{6.6.6}$$

Morphological operations (6.6.5-6) greatly resemble linear convolution. Definitions (6.6.5-6) are of great practical importance since they introduce a method of numerical computation of erosion and dilation. Definitions (6.6.5-6) can be greatly simplified when the structuring function $g(x)$ is of the form (6.6.1):

$$[f \oplus G^s](x) = [f \oplus g^s](x) = \max_{\substack{z \in D \\ z-x \in G}} \{f(z)\} \tag{6.6.7}$$

$$[f \ominus G^s](x) = [f \oplus g^s](x) = \min_{\substack{z \in D \\ z-x \in G}} \{f(z)\} \tag{6.6.8}$$

The grayscale erosion $f \ominus G^s$ and dilation $f \oplus G^s$ are called *erosion* and *dilation of function by set* [1].

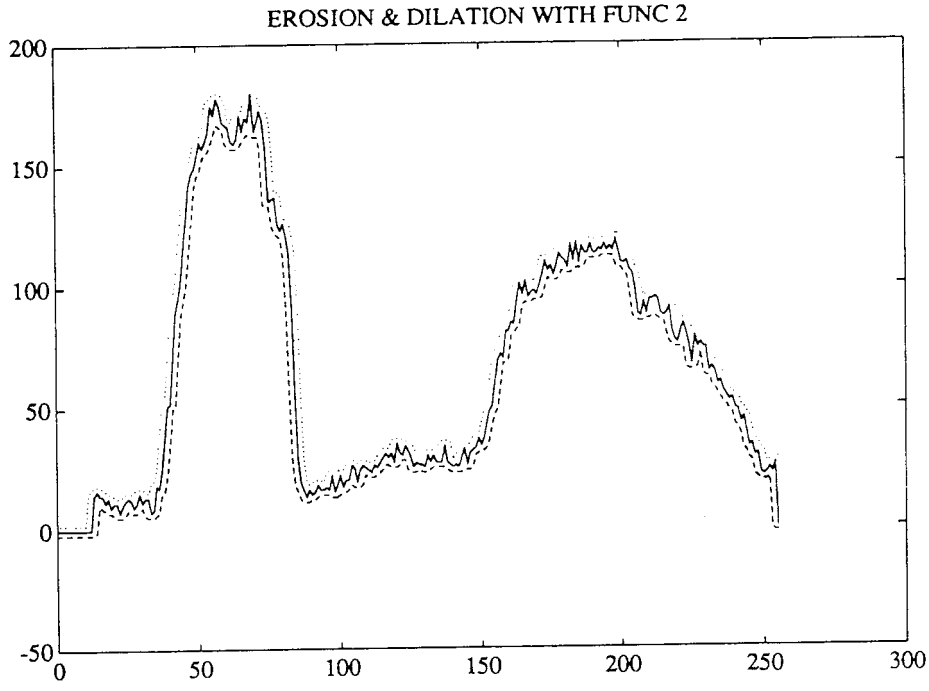
EROSION & DILATION WITH FUNC 2
200
150
100
50
0
-50
0
50
100
150
200
250
300

(a)

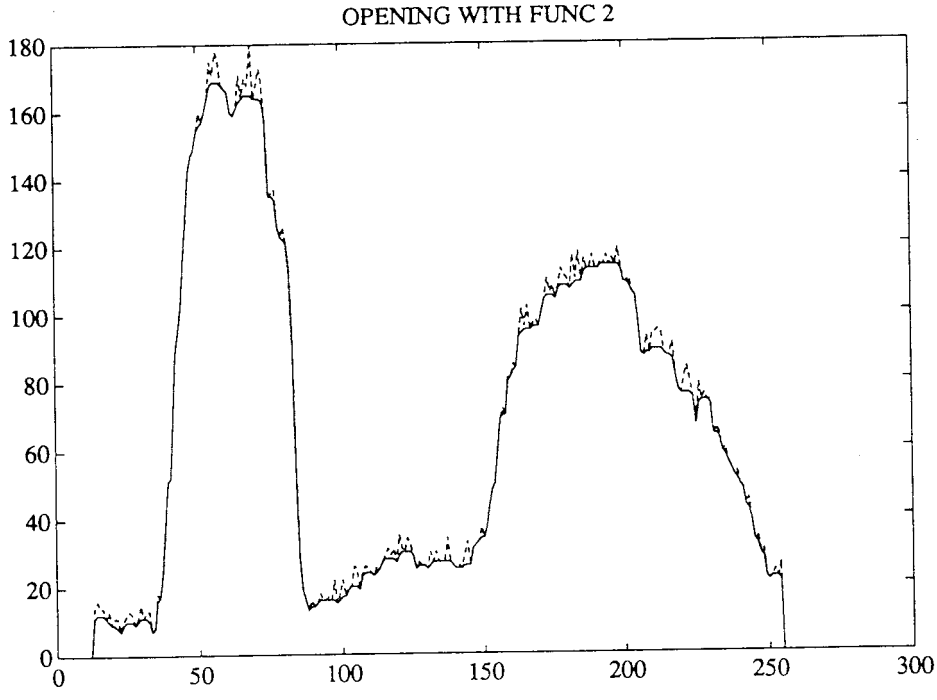
OPENING WITH FUNC 2
180
160
140
120
100
80
60
40
20
0
0
50
100
150
200
250
300

(b)

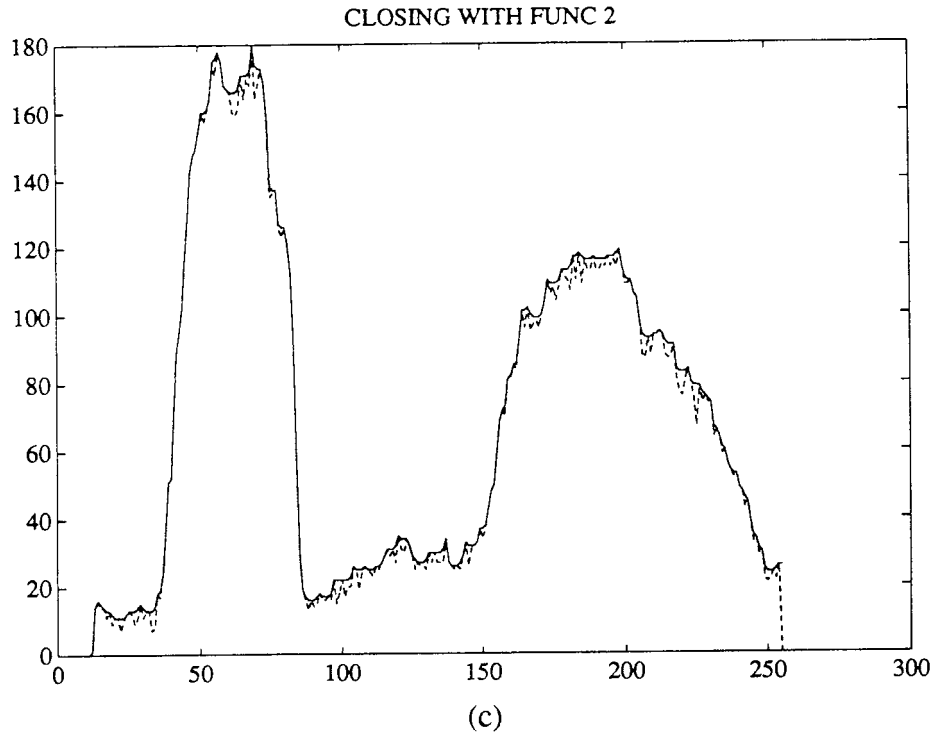

Figure 6.6.1: (a) The original function is denoted by the solid line, whereas its dilation and erosion by a 5-point structuring function are denoted by dotted and dashed lines respectively; (b) Opening of the original function (solid line); (c) Closing of the original function (solid line).

If the domain $D=\mathbf{Z}$ and the domain G is a subset of $\mathbf{Z}$:

$$G = \{-\nu,...,0,...,\nu\} = G^s$$

the erosion and dilation of function by set are given by:

$$[f \oplus G^s](i) = \max\{f(i-\nu),...,f(i),...,f(i+\nu)\} \tag{6.6.9}$$

$$[f \ominus G^s](i) = \min\{f(i-\nu),...,f(i),...,f(i+\nu)\} \tag{6.6.10}$$

Therefore, they are completely equivalent to the n-th ranked order filter and to the 1st ranked-order filter, respectively ($n=2\nu+1$), which are analyzed in chapter 5. An example of such an erosion and dilation is shown in Figure 6.6.1. The structuring function used has a 5-point domain $G=\{-2,-1,0,1,2\}$.

Grayscale erosion and dilation possess similar properties to the binary erosion and dilation. They are presented here without proof, since their proofs are very simple and can be based on the corresponding properties of the binary operators [41],[1, p.442]:

(1)	Commutativity	$f \oplus g = g \oplus f$	(6.6.11)
(2)	Associativity	$f \oplus (g \oplus k) = (f \oplus g) \oplus k$	(6.6.12)
(3)	Distributivity	$(f \vee g) \oplus h = (f \oplus h) \vee (g \oplus h)$	(6.6.13)
		$(f \wedge g) \ominus h = (f \ominus h) \wedge (g \ominus h)$	(6.6.14)
(4)	Parallel composition	$f \ominus (g \vee h) = (f \ominus g) \wedge (f \ominus h)$	(6.6.15)
(5)	Serial composition	$f \oplus (g \oplus h) = (f \oplus g) \oplus h$	(6.6.16)
		$f \ominus (g \oplus h) = (f \ominus g) \ominus h$	(6.6.17)
(6)	Umbra homomorphism	$U[f \oplus g] = U[f] \oplus U[g]$	(6.6.18)
		$U[f \ominus g] = U[f] \ominus U[-g]^c$	(6.6.19)

Umbra homomorphism is a very important property from a theoretical point of view because it links grayscale morphology with umbrae and binary morphology. Serial composition is another important property of grayscale erosion and dilation because it can be used for its fast implementation when a structuring function can be decomposed to simpler ones of the form:

$$g = g_1 \oplus g_2 \oplus \cdots \oplus g_k \tag{6.6.20}$$

In this case, erosion and dilation become:

$$f \oplus g = (\ldots((f \oplus g_1) \oplus g_2) \oplus \cdots \oplus g_k) \tag{6.6.21}$$

$$f \ominus g = (\ldots((f \ominus g_1) \ominus g_2) \ominus \cdots \ominus g_k) \tag{6.6.22}$$

Grayscale erosion and dilation are dual operations. Their duality is expressed by the following relation:

$$f \ominus g^s = -[(-f) \oplus g^s] \tag{6.6.23}$$

Proof:

$$-[(-f) \oplus g^s](x) = -\max_{\substack{z \in D \\ z-x \in G}} \{-f(z) + g(z-x)\}$$

$$= \min_{\substack{z \in D \\ z-x \in G}} \{f(z) - g(z-x)\} = [f \ominus g^s](x)$$

Another set of dual operations is grayscale opening:

$$f_g(x) = [(f \ominus g^s) \oplus g](x) = [f(x) \ominus g(-x)] \oplus g(x) \tag{6.6.24}$$

and grayscale closing:

$$f^g(x) = [(f \oplus g^s) \ominus g](x) = [f(x) \oplus g(-x)] \ominus g(x) \tag{6.6.25}$$

Lantuejoul and Serra [11] introduced the name *M-filters* for grayscale opening and closing. We shall use instead the term *morphological filters* to avoid any confusion with the M-estimators and M-filters described in chapters 2 and 5.
If $g(x)$ is a structuring function of the form (6.6.1), (6.6.24-25) are equivalent to opening and closing of function by set:

$$f_G(x) = [(f \ominus G^s) \oplus G](x) \tag{6.6.26}$$

$$f^G(x) = [(f \oplus G^s) \ominus G](x) \tag{6.6.27}$$

An example of such openings and closings for $G=\{-2,-1,0,1,2\} \in \mathbf{Z}$ is shown in Figure 6.6.1.

Opening is antiextensive, whereas closing is extensive. Thus, if $g(0)>0$ [41]:

$$f \ominus g \le f_g \le f \le f^g \le f \oplus g \tag{6.6.28}$$

Furthermore, opening and closing are:

(1)	translation invariant	$(f_g)(x-t)=[f(x-t)]_g$	(6.6.29)
		$(f^g)(x-t)=[f(x-t)]^g$	(6.6.30)
(2)	increasing	$f_1 \le f_2 \Rightarrow (f_1)_g \le (f_2)_g$	(6.6.31)
		$f_1 \le f_2 \Rightarrow (f_1)^g \le (f_2)^g$	(6.6.32)
(3)	idempotent	$(f_g)_g = f_g$	(6.6.33)
		$(f^g)^g = f^g$	(6.6.34)

The proof of translation invariance is very simple. The proofs of increasing property and idempotence are omitted because they are similar to the proofs of (6.3.7-12).

Finally, the duality theorem for opening and closing can be stated as follows:

$$-f_g = (-f)^g \tag{6.6.35}$$

$$f^g = -(-f)_g \tag{6.6.36}$$

Proof:

$$-f_g = -[(f \ominus g^s) \oplus g] = [-(f \ominus g^s)] \ominus g = [(-f) \oplus g^s] \ominus g = (-f)^g$$

A function f is called *open with respect to* g if and only if $f=f_g$. Likewise, f is called closed with respect to g iff $f=f^g$. Thus f is open, if it is a root of the opening transformation. It is closed, if it is a root of the closing transformation. The following theorem gives the roots of opening and closing [41].

Theorem 6.6.1: A function f is open (respectively, closed) with respect to a function g if and only if $f=h \oplus g$ (respectively $f=h \ominus g$) where h is an arbitrary function.

The proof is omitted because it is similar to the proof of Proposition 1 (section 6.3). The threshold decomposition described in chapter 4 can also be applied to the grayscale morphological operations and used for their fast implementation [58].

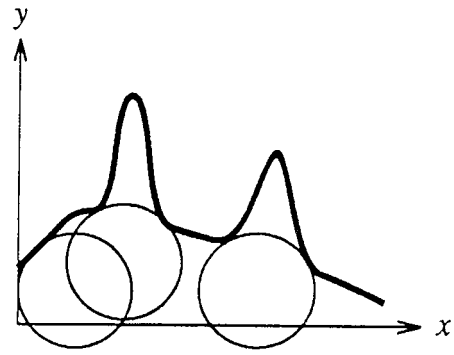

Figure 6.6.2: Rolling ball transformation.

(a)

(b)

(c)

(d)

(e) (f)

Figure 6.6.3: (a) Original image; (b) Erosion by a 3×3 structuring set; (c) Dilation by a 3×3 structuring set; (d) Difference between the original image and the eroded image; (e) Opening by a 3×3 structuring set; (f) Closing by a 3×3 structuring set.

Opening and closing are the basis of the definitions of morphological filters. Therefore it would be interesting to give a graphical representation of their operation. An 1-d grayscale function is shown in Figure 6.6.2. The opening is essentially a rolling ball transformation. The rolling ball exactly traces the smoothly varying contours, where positive impulses exist the rolling ball deletes them, and where negative impulses exist, the rolling ball leaves gaps. The effect of the closing is exactly opposite to that of opening: it deletes negative impulses and broadens the positive ones. An example of erosion, dilation, opening and closing of a gray-valued image with a 3×3 structuring set is shown in Figure 6.6.3. It is clearly seen that erosion broadens the image black region (see the girl's eyes) because of the min operator used in (6.6.6), whereas dilation broadens the image bright regions because of the max operator used in (6.6.5).

6.7 MORPHOLOGICAL FILTERS

Morphological filters are nonlinear filters based on morphological transformations of functions by sets. Such filters are the grayscale erosion and dilation, defined by (6.6.7-8) and the opening and closing of a function by set defined (6.6.26-27). Furthermore, another set of morphological filters studied in the literature [19,41,42] are the *close-opening (CO)* and the *open-closing (OC) filters:*

$$y = [(f^G)_G](x) \tag{6.7.1}$$

$$y = [(f_G)^G](x) \tag{6.7.2}$$

where f_G, f^G are given by (6.6.26-27). If $f(x)$ is a sampled function and $f_i = f(i)$, $i \in \mathbf{Z}$ and G is the structuring set (6.6.8) the output of one-dimensional erosion and dilation filters is given by (6.6.9-10):

$$y_i = [f \oplus G^s](i) = \max\{f_{i-v},\ldots,f_i,\ldots,f_{i+v}\} \tag{6.7.3}$$

$$y_i = [f \ominus G^s](i) = \min\{f_{i-v},\ldots,f_i,\ldots,f_{i+v}\} \tag{6.7.4}$$

These two filters will not be studied further here because they correspond to ranked-order filters, whose study is included in chapter 5. Opening and closing are two-step operations. Therefore, the output of the one-dimensional opening filter is given by

$$y_i = f_G(i) = \max\{f_{i-v}^{(1)},\ldots,f_i^{(1)},\ldots,f_{i+v}^{(1)}\} \tag{6.7.5}$$

$$f_i^{(1)} = \min\{f_{i-v},\ldots,f_i,\ldots,f_{i+v}\} \tag{6.7.6}$$

Similarly, the one-dimensional closing filter is defined as:

$$y_i = \min\{f_{i-v}^{(1)},\ldots,f_i^{(1)},\ldots,f_{i+v}^{(1)}\} \tag{6.7.7}$$

$$f_i^{(1)} = \max\{f_{i-v},\ldots,f_i,\ldots,f_{i+v}\} \tag{6.7.8}$$

The one-dimensional close-opening filter is a four-step operation:

$$y_i = [(f^G)_G](i) = \max\{f_{i-v}^{(3)},\ldots,f_i^{(3)},\ldots,f_{i+v}^{(3)}\} \tag{6.7.9}$$

$$f_i^{(3)} = \min\{f_{i-v}^{(2)},\ldots,f_i^{(2)},\ldots,f_{i+v}^{(2)}\} \tag{6.7.10}$$

$$f_i^{(2)} = \min\{f_{i-v}^{(1)},\ldots,f_i^{(1)},\ldots,f_{i+v}^{(1)}\} \tag{6.7.11}$$

$$f_i^{(1)} = \max\{f_{i-v},\ldots,f_i,\ldots,f_{i+v}\} \tag{6.7.12}$$

The definition of an open-closing filter is the same as (6.7.9-12) if the max and min operators interchange positions.

Morphological filters possess certain nice syntactic and statistical properties, which are related to the corresponding properties of the median filter. Let A be the window set of the median filter having size $n=2v+1$ and let $m=v+1$ be the size of the set G. Let $\text{med}(f;A)$ denote the median filtered sequence. This sequence is bounded from below and above by opening and closing, respectively [42]:

Proposition 6.7.1:

$$f_G \le \text{med}(f;A) \le f^G \tag{6.7.13}$$

$$X_G \le \text{med}(X;A) \le X^G \tag{6.7.14}$$

where $\text{med}(X;A)$ denotes the binary median filtering of a binary sequence X

(i.e., of a binary set).
The property 6.7.1 is very important because it can be used to find a relation between the roots of one-dimensional OC and CO filters and those of the median filter [42]:
Proposition 6.7.2: A set X or a function f, of finite extent, is a median root with respect to A, iff it is a root of both opening and the closing by G.
Let us define by $\text{med}^n(f;A)$ the output of a median filter iterated n times and by $\text{med}^\infty(f;A)$ the median root. It can be proven that the median root is bounded by close-opening and open-closing [42]:
Proposition 6.7.3:

$$(f_G)^G \leq \text{med}^\infty(f;A) \leq (f^G)_G \tag{6.7.15}$$

$$(X_G)^G \leq \text{med}^\infty(X;A) \leq (X^G)_G \tag{6.7.16}$$

The outputs of the CO and OC filters are median roots themselves [42]:
Proposition 6.7.4: The open-closing and the close-opening by G of any signal f of finite extent are median roots with respect to A. That is:

$$(f_G)^G = \text{med}[(f_G)^G;A] \tag{6.7.17}$$

$$(f^G)_G = \text{med}[(f^G)_G;A] \tag{6.7.18}$$

Proposition 6.7.4 is a very important practical result since it can give a median root in just one pass.

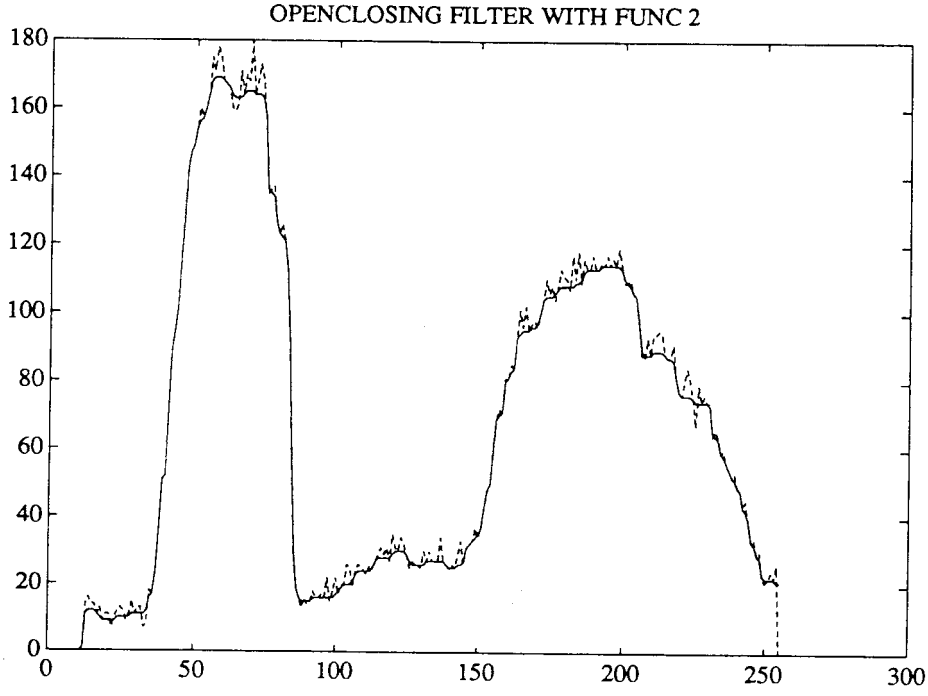

(a)

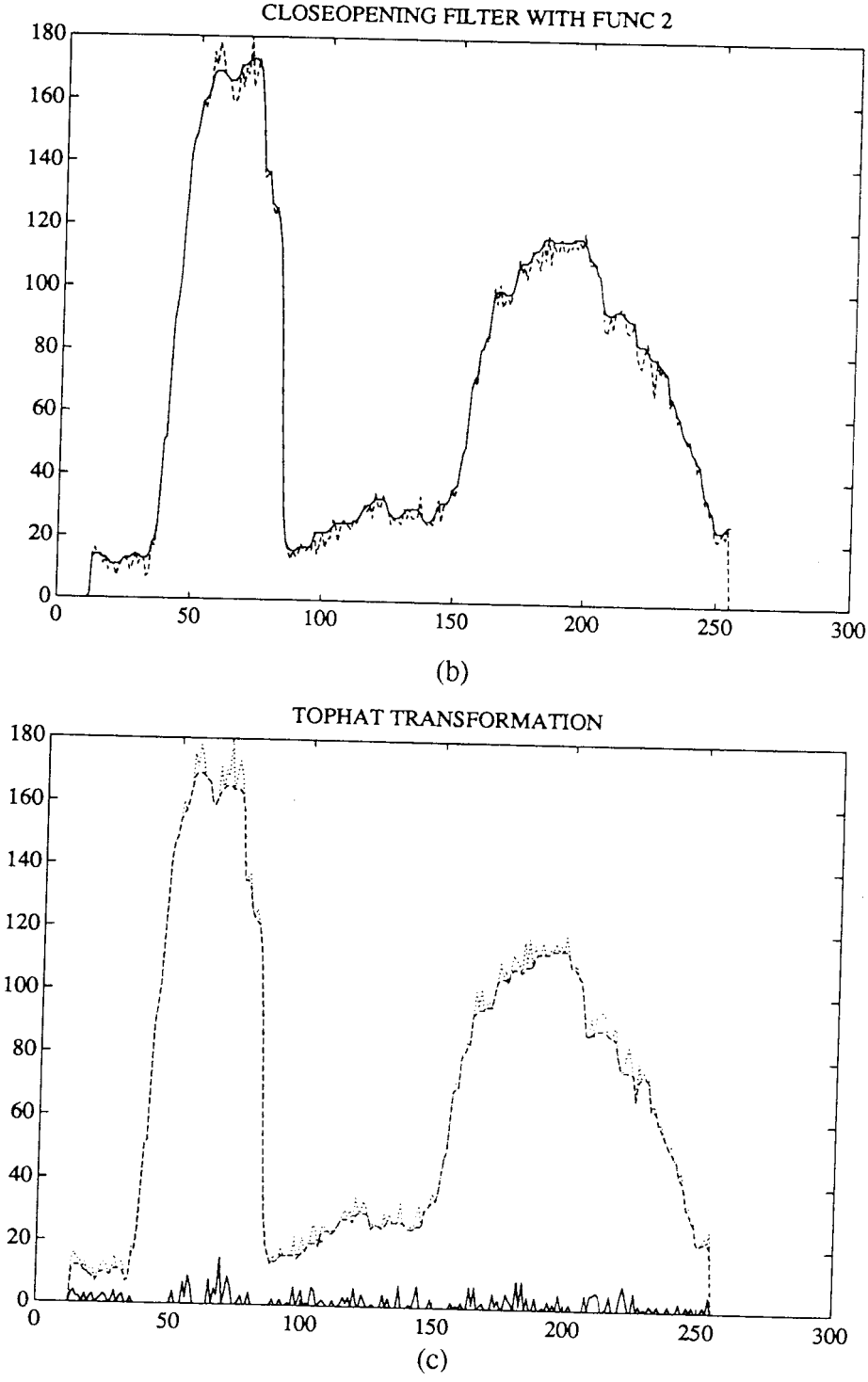

Figure 6.7.1: (a) Open-closing of the function shown in Figure 6.6.1a; (b) Close-opening of the function shown in Figure 6.6.1a; (c) Top-hat transformation of the function shown in Figure 6.6.1a.

An example of one-dimensional 3-point OC and CO filtering is shown in Figure 6.7.1. The median root has also been obtained by using a median filter having window size 5 in four iterations. The bounds of proposition 6.7.3 are satisfied. However, the difference between the median root and the open-closing and close-opening is very small. Thus the median root is not displayed.

A statistical analysis of the morphological filters is presented in [19]. The output distributions of the close-opening and open-closing filters are given by:

$$F_{CO}(y) = mF(y)^m - (m-1)F(y)^{m+1} + F(y)^{2m}(1-F(y)) + \frac{(m+1)m}{2} F(y)^{2m}(1-F(y))^2 \quad (6.7.19)$$

$$F_{OC}(y) = 1 - [m(1-F(y))^m - (m-1)(1-F(y))^{m+1} + (1-F(y))^{2m}F(y) + \frac{m(m+1)}{2} (1-F(y))^{2m}F(y)^2] \quad (6.7.20)$$

for $m=v+1$

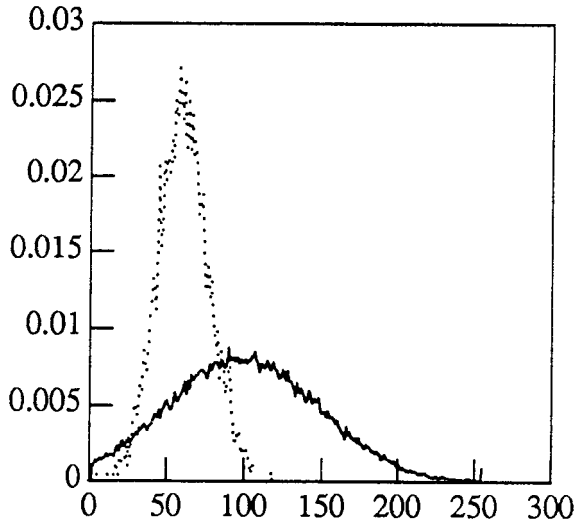

Figure 6.7.2: Gaussian probability input distribution having mean at 100 (solid curve) and the probability distribution of the output of a 3×3 openclosing filter (dotted curve). The shift of the output mean to smaller values is evident.

The proofs are rather lengthy and they are omitted here. $F(y)$ is the probability distribution of the input signal. The output pdf of a 3×3 two-dimensional OC filter having Gaussian input density is shown in Figure 6.7.2. It is seen that the output of the OC filter is strongly biased toward small output values. This is explained by the min operator in (6.7.12). The output density function of the

CO filter is not plotted because it is the symmetric of the pdf of the OC filter output. The output of the CO filter is biased toward large output values. The morphological filters can be easily extended to two dimensions with respect to a two dimensional structuring set G. However, in this case, propositions similar to 6.7.1 and 6.7.2 are not valid in general for any structuring element.

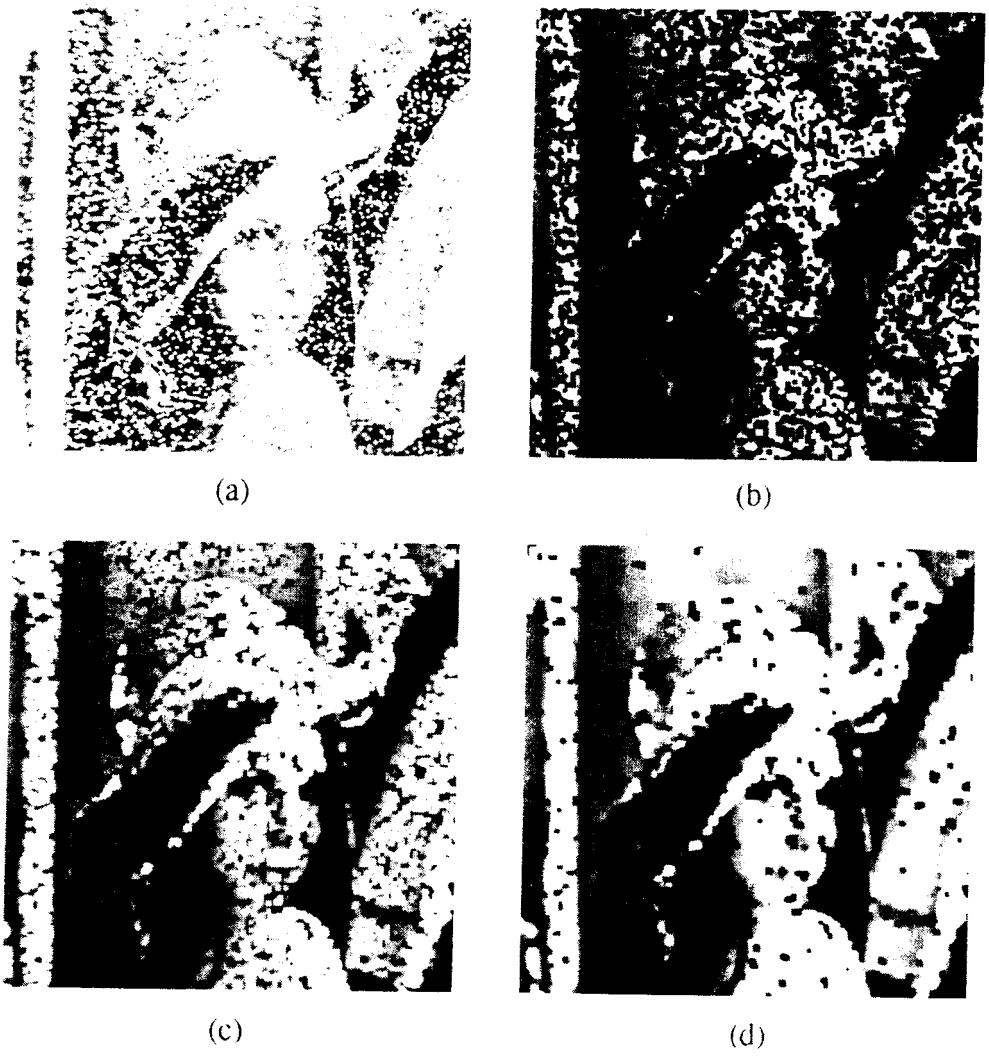

Figure 6.7.3: (a) Original image corrupted by 10% mixed impulsive noise; (b) Output of the erosion by a 3×3 structuring set; (c) Output of the opening by a 3×3 structuring set; (d) Output of the OC filter by a 3×3 structuring set.

An example of two-dimensional OC filtering (6.7.1), by using a 3×3 square structuring set, is shown in Figure 6.7.3. Image 6.7.3a is corrupted by 10%

salt-pepper noise. The opening operation of the OC filter removes positive impulses but enhances the negative ones. This mode of operation is easily explained by the opening definition (6.7.5-6). The min operator in (6.7.6) suppresses any positive impulse. Most of the negative impulses are removed by the closing operation of the OC filter. However, the negative impulses have already been enhanced by opening. Therefore, some negative impulses remain in the OC filtered image. In contrast, some positive impulses can remain in an CO filtered image. The OC filter can be compared to the 3×3 median filter by comparing Figures 6.7.3d and 4.7.1c. Clearly, the median filter has superior performance in the salt-pepper noise filtering than the OC filter.

Digital filters based in morphological operations have also been used in impulsive noise filtering and background normalization of ECG signals [72]. Morphological filters can also be used for edge detection. The following morphological filter:

$$y = f(x) - [f \ominus B](x) \tag{6.7.21}$$

has been proposed [10] as a robust edge detector. It has also been found that this morphological edge detector is more robust than other linear edge detection schemes. An example of the performance of this edge detector is shown in Figure 6.6.3d. An extension of this edge detector is the following:

$$y = f(x) - [f \ominus nB](x) \tag{6.7.22}$$

where the structuring set nB is defined as:

$$nB = B \oplus B \oplus \cdots \oplus B \quad (n \text{ times}) \tag{6.7.23}$$

and the symbol - in (6.7.22) denotes algebraic difference. Parameter n controls the thickness of the edges, i.e., the larger n, the thicker the edges. The orientation of B controls the orientation of the edges. Other morphological edge detectors are presented in [63-65].

The opening f_{nB} of a function is a low-pass nonlinear filter, because it destroys the high frequencies of an image, as has already been shown by the illustrative rolling ball interpretation shown in Figure 6.6.2. Therefore, the following filter, called *top-hat transformation* [20], is a high-pass filter:

$$y = f(x) - f_{nB}(x) \tag{6.7.24}$$

The opening f_{nB} erases all peaks in which the structuring element nB cannot enter. Therefore, only those peaks appear in $f - f_{nB}$, and the background is eliminated as it is seen in Figure 6.7.1c. Combinations of top-hat transformations by anisotropic structuring elements have been used for cleaning images from astronomy [22]. The top-hat transformation has also been used to find galaxies in astronomical images [11].

6.8 MORPHOLOGICAL SKELETONS

Mathematical morphology is very rich in providing means for the representation and analysis of binary and grayscale images. The morphological representation of images is very well suited for the description of the geometrical properties of the image objects. Therefore, it can be used for pattern recognition, robotic vision, image coding, etc.

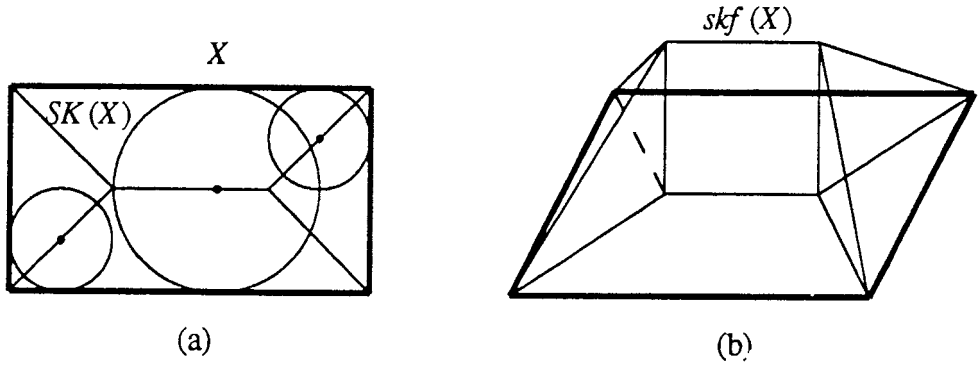

Figure 6.8.1: (a) Skeleton of a rectangle; (b) Skeleton function of the rectangle.

One of the most important morphological representation schemes is the *skeleton* of an image, shown in Figure 6.8.1. The idea of transforming an image to a skeleton is due to Blum [25,26], who called it *medial axis*. Blum's initial procedure to obtain the medial axis was to set up *grass fires* along the object boundary, simultaneously at $t=0$, and to let the fire wavefronts to propagate toward the image object center by Huygen's principle at uniform speed. The medial axis consists of those points, where the fire wavefronts intersect and extinguish, together with their arrival times, which constitute the *medial axis function*. Blum tried to relate this grass fire propagation mechanism to a hypothesized brain mechanism of shape recognition in animal vision. Subsequently, a mathematical theory for the skeletons of continuous images [27,28] and for discrete images [29, 30, 31] has been developed. In reviewing the previous research, Blum [26] showed that the medial axis is the locus of the centers of the *maximal discs* inscribable inside an image object. Lantuejoul [32,33] connected skeletons with mathematical morphology and proved that skeletons can be obtained by morphological transformations. Such a skeleton will be called *morphological*, to be distinguished from skeletons obtained by other mathematical descriptions, because there are some differences in the various skeleton definitions. These differences are discussed in [1, p. 382].

In this section the definition of the skeleton of binary images will be given first and it will be generalized subsequently for graytone images. Let X be an image object in $\mathbf{R}^2$. The skeleton $SK(X)$ is the set of the centers of the maximal inscribable disks inside X. Such a disk is maximal if it is not properly contained in any other disk totally included in X. A maximal disk touches the object boundary in at least two different points. This definition of the skeleton is exemplified in Figure 6.8.1. Each point of the skeleton is associated with the radius r of the corresponding maximal disk. Therefore, a function $skf(z)$ can be defined, whose domain is $SK(X)$ and which takes values in $\mathbf{R}$:

$$z \in SK(X) \rightarrow skf(z) \in \mathbf{R} \tag{6.8.1}$$

This function is called *skeleton function* or *quench function*. Let us denote by $S_r(X)$ the subset of $SK(X)$ whose points correspond to centers of maximal inscribable disks having the same radius $r>0$. Lantuejoul [33] has proven that the morphological skeleton is given by:

$$SK(X) = \bigcup_{r>0} S_r(X) = \bigcup_{r>0} [(X \ominus rB) - (X \ominus rB)_{drB}] \tag{6.8.2}$$

where rB denotes an open disk of radius r and drB denotes a closed disk of infinitesimally small radius dr. This process is illustrated in Figure 6.8.2.

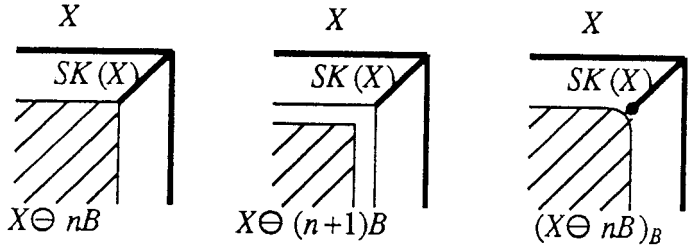

Figure 6.8.2: Illustration of the skeletonization process.

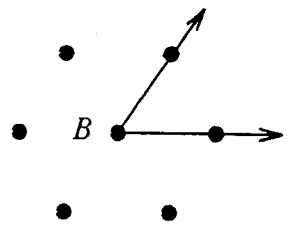

Figure 6.8.3: Symmetric hexagonal structuring element of radius 1 on the hexagonal grid.

The transition from the skeleton definition (6.8.2) in $\mathbf{R}^n$ to the skeleton in $\mathbf{Z}^n$ is quite troublesome. The major problem is the approximation of the disks rB and drB in the grid $\mathbf{Z}^n$. In a hexagonal grid, the circle can be approximated by the symmetric hexagon shown in Figure 6.8.3. This seven pixel structuring set can be said to have a *discrete radius* $n=1$. The element nB:

$$nB = B \oplus B \oplus \cdots \oplus B \quad (n \text{ times}) \tag{6.8.3}$$

has discrete radius n. By using the hexagon structuring element, Serra [1, p. 389] provided the following algorithm for the morphological skeleton on a hexagonal grid:

$$S_n(X) = (X \ominus nB^s) - (X \ominus nB^s)_B \qquad n=0,1,2,...,N \tag{6.8.4}$$

$$SK(X) = \bigcup_{n=0}^{N} S_n(X) \tag{6.8.5}$$

The discrete binary object X can be reconstructed exactly from its discrete skeleton as follows:

$$X = \bigcup_{n=0}^{N} [S_n(X) \oplus nB] \tag{6.8.6}$$

However, hexagonal grids are of limited use. Therefore, Maragos [24] proposed the use of definitions (6.8.4-6) for the rectangular grid. In this grid the closest approximation to the circle of discrete radius one is the SQUARE structuring element. A better approximation of the circle is the CIRCLE structuring element shown in Figure 6.2.4. Its discrete radius is 2. A skeleton obtained by using the CIRCLE is shown in Figure 6.8.4.

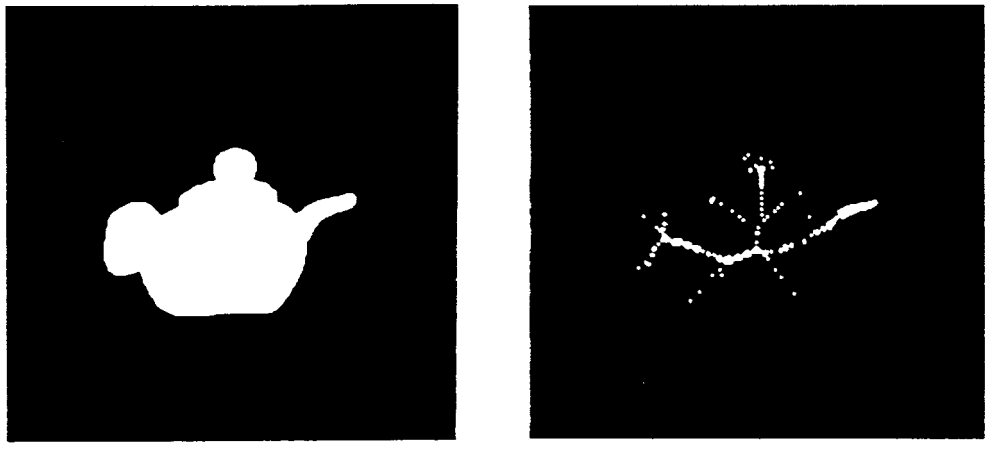

(a) (b)

Figure 6.8.4: (a) Object POT; (b) Skeleton of POT obtained by using the CIRCLE.

Furthermore, Maragos [24] proposed a serial decomposition of (6.8.4-6.8.5) for the fast calculation of the skeleton:

$$S_0(X) = X - X_B \tag{6.8.7}$$

$$S_1(X) = (X \ominus B^s) - (X \ominus B^s)_B \tag{6.8.8}$$

$$\vdots$$

$$S_N(X) = [(X \ominus (N-1)B^s) \ominus B^s] - [X \ominus (N-1)B^s]_B \tag{6.8.9}$$

Definition (6.8.4) is fully equivalent to (6.8.7-9) if the distributivity property (6.2.36) is considered. A similar serial decomposition of the reconstruction procedure (6.8.6) is given by:

$$X = [...[[S_N(X) \oplus B \cup S_{N-1}(X)] \oplus B] \cup S_{N-2}(X)...] \oplus B \cup S_0(X) \tag{6.8.10}$$

The fast skeletonization and reconstruction procedures are shown in Figure 6.8.5.

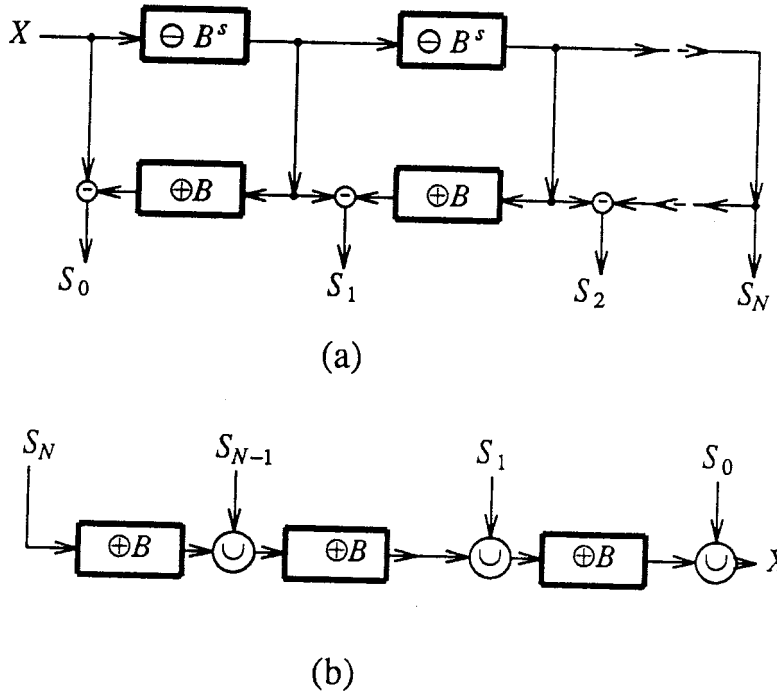

Figure 6.8.5: (a) Fast skeletonization process; (b) Fast object reconstruction from skeleton subsets (adapted from [24]).

Partial reconstructions of X can be obtained if only the $N-k$ skeleton subsets $S_n(X)$, $n=k,...,N$ are used:

$$X' = \bigcup_{n=k}^{N} S_n(X) \oplus nB \tag{6.8.11}$$

The result of the partial reconstruction (6.8.11) is the opening of X by kB, X_{kB} [24]:

$$X_{kB} = (X \ominus kB^s) \oplus kB = \left[\left[\bigcup_{n=0}^{N} S_n(X) \oplus nB \right] \ominus kB^s \right] \oplus kB$$

$$= \left[\bigcup_{n=k}^{N} S_n(X) \oplus (n-k)B \right] \oplus kB = X'$$

Also eroded versions of X of the form $X \ominus kB^s$ can be obtained from the partial reconstruction of X:

$$X \ominus kB^s = \bigcup_{n=k}^{N} [S_n(X) \oplus (n-k)B] \tag{6.8.12}$$

if the disks of size n are substituted with disks of size $n-k$. A dilated version of X can also be obtained from its skeleton:

$$X \oplus kB^s = \bigcup_{n=0}^{N} [S_n(X) \oplus (n+k)B] \tag{6.8.13}$$

if the disks of size n are replaced with disks of size $n+k$. If some skeleton subsets $S_n(x)$, $0 \le n \le k$ are omitted and the result of the reconstruction is dilated, the original object X cannot be reconstructed:

$$X' = \bigcup_{n=k}^{N} [S_n(X) \oplus (n+k)B] \neq X$$

This result is important in image coding applications because it states that the loss of some fine details described by $S_n(X)$, $0 \le n \le k$ cannot be compensated by a final dilation.

Morphological skeletons of binary images possess certain interesting properties [1,24]:

Proposition 6.8.1: Skeletons are translation invariant.

Proposition 6.8.2: Skeletons in the Euclidean space $\mathbf{R}^2$ are invariant in the change of scale.

Proposition 6.8.3: The mapping $X \to \overline{SK(X)}$ is lower semicontinuous, i.e., very

point x of $\overline{SK(X)}$ is a limit of a sequence of points x_i with $x_i \in SK(X_i)$. $\overline{SK(X)}$ is the adherence of $SK(X)$ [1, p.378].

The definition of adherent points is given in section 6.1. Note that $\overline{SK(X)}$ is not upper-semicontinuous transformation, which is a requirement to be a morphological transformation.

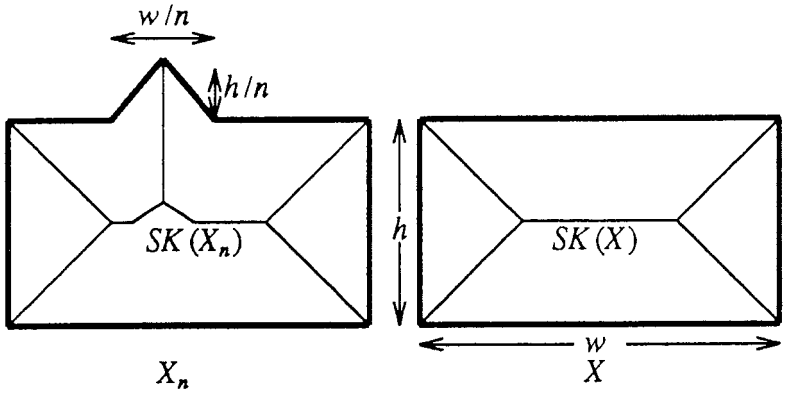

Figure 6.8.6: Illustration of the continuity properties of skeleton (adapted from [53]).

The poor continuity properties of skeleton are depicted in Figure 6.8.6. A rectangle has a small bump of height h/n and width w/n. This bump causes a disturbance to the skeleton of the rectangle. When n tends to infinity the bump disappears. However, the transition in the skeleton is not continuous. Furthermore, skeleton requires global knowledge for its computation. Thus *it is not* a morphological transformation and it is sensitive to noise, especially to small holes in an image object.

Proposition 6.8.4: Skeleton is antiextensive (if $\{0\} \in B$), translation-invariant, and idempotent.

Proposition 6.8.5:

$$\text{If } |B| = 1 \Rightarrow SK(X) = \varnothing$$

$$\text{If } X \ominus B^s = \varnothing \Rightarrow SK(X) = X$$

This property is important because it shows that any zero thickness set is a skeleton itself.

Proposition 6.8.6: If $SK(X)$ is the skeleton of X using B as a structuring element, then B_z gives $[SK(X)]_{-z}$ as the skeleton of X.

Proposition 6.8.7: The skeleton subsets are disjoint.

Proposition 6.8.8: If the skeleton has been obtained by using a convex and bounded structuring element B, $(nB)_z$ is the maximal inscribable structuring element in X, iff $z \in S_n(X)$.

Proposition 6.8.9: If B is bounded and convex, X is equal to X_{kB} iff $S_n(X) = \varnothing$, $n=0,1,..,k-1$.

Proposition 6.8.8 is important because it justifies the fact that the skeleton given by (6.8.4-5) is the locus of the centers of the maximal inscribable disks in X. Proofs of all previously mentioned properties can be found in [24,53].

Skeletons defined by (6.8.4-6) over a rectangular grid are translation and scale invariant but not rotation invariant, even in the case when the CIRCLE structuring element is employed. Therefore, a generalized definition of skeletons has been proposed [43] to accommodate rotation invariance:

$$SK(X) = \bigcup_{n=0}^{N} S_n(X) \tag{6.8.14}$$

$$S_n(X) = (X \ominus B(n)^s) - (X \ominus B(n)^s)_{B_n(1)}$$

$$N = \max\{n : X \ominus B(n) \neq \varnothing\}$$

where $B(n)$ is a structuring element of size n and $B_n(1)$ is a structuring element related to $B(n)$ and having size 1. Several skeleton subclasses can be derived from (6.8.14) by specifying the types of structuring elements $B(n)$, $B_n(1)$ used. For example, if $B(n)$ is equal to nB of (6.8.3) and $B_n(1)=B$, the skeleton definition (6.8.4) results. If a multitude of structuring elements is used, the structuring element of size n can be defined as follows:

$$B(n) = \begin{cases} B_1 \oplus B_2 \oplus \cdots \oplus B_m & n \le m \\ pB(m) \oplus B(q) & n = pm+q > m \ , \ q < m \end{cases} \tag{6.8.15}$$

$$B_n(1) = \{B_i : \ i = (n-1) \bmod m + 1\}$$

The resulting skeleton (6.8.14) is the so-called *periodic uniform-step distance (PUSD) skeleton*. PUSD skeleton is more isotropic than the original skeleton (6.8.4), if the structuring elements are chosen properly [43]. If the structuring

elements in (6.8.15) are chosen in such a way that they approximate a disk, the resulting skeleton (6.8.14) is approximately rotation invariant and it is called *pseudo-Euclidean skeleton*. A systematic method to generate quasi-circular structuring elements of all sizes has been found [52]. They can always be decomposed into small structuring elements of size 2 or 3 pixels, as is seen in Figure 6.8.7. Therefore, the computation of the pseudo-Euclidean skeleton can be done in a way similar to the one described by (6.8.7-9). An example of the rotation invariance properties of the pseudo-Euclidean skeleton is shown in Figure 6.8.8. Figures 6.8.8a and 6.8.8b show the skeleton (6.8.4) and the pseudo-Euclidean skeleton, respectively, of an airplane figure. The skeletons of the airplane figure rotated by 210 degrees is shown in Figures 6.8.8c and 6.8.8d, respectively. The pseudo-Euclidean skeleton shows better rotation invariance than the classical skeleton definition (6.8.4).

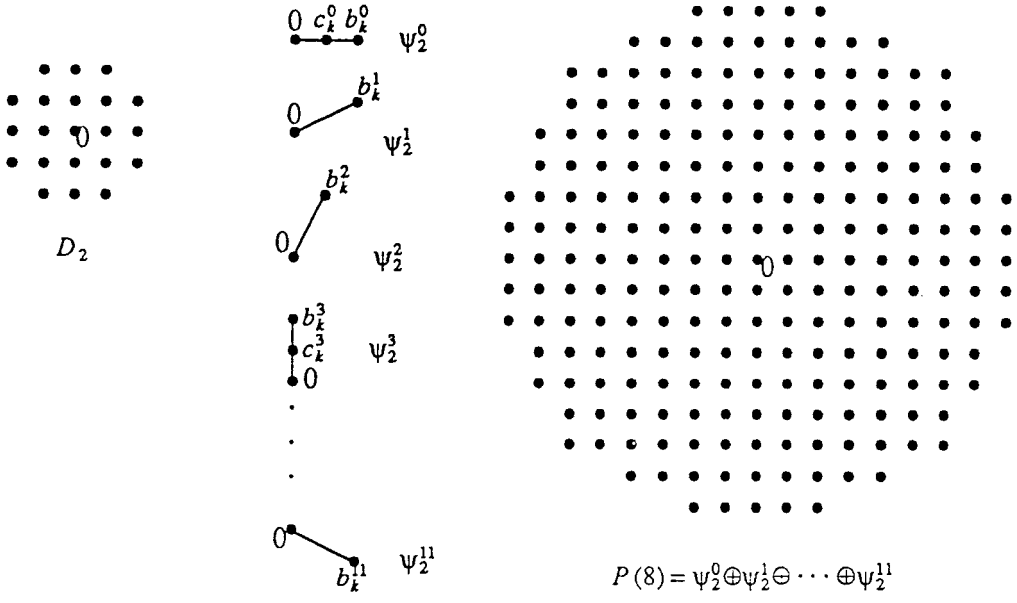

Figure 6.8.7: Decomposition of a disk of size 8 to structuring sets having size 2 or 3 pixels.

Sometimes skeletons carry more information for an object than what is needed for certain applications e.g., for object recognition. In those cases it is possible to do only partial object reconstruction by discarding some skeleton subsets that describe either details or object regions which are also described by

other skeleton subsets having larger skeleton values. Such a partial object reconstruction is shown in Figure 6.8.9 for the airplane figure [44].

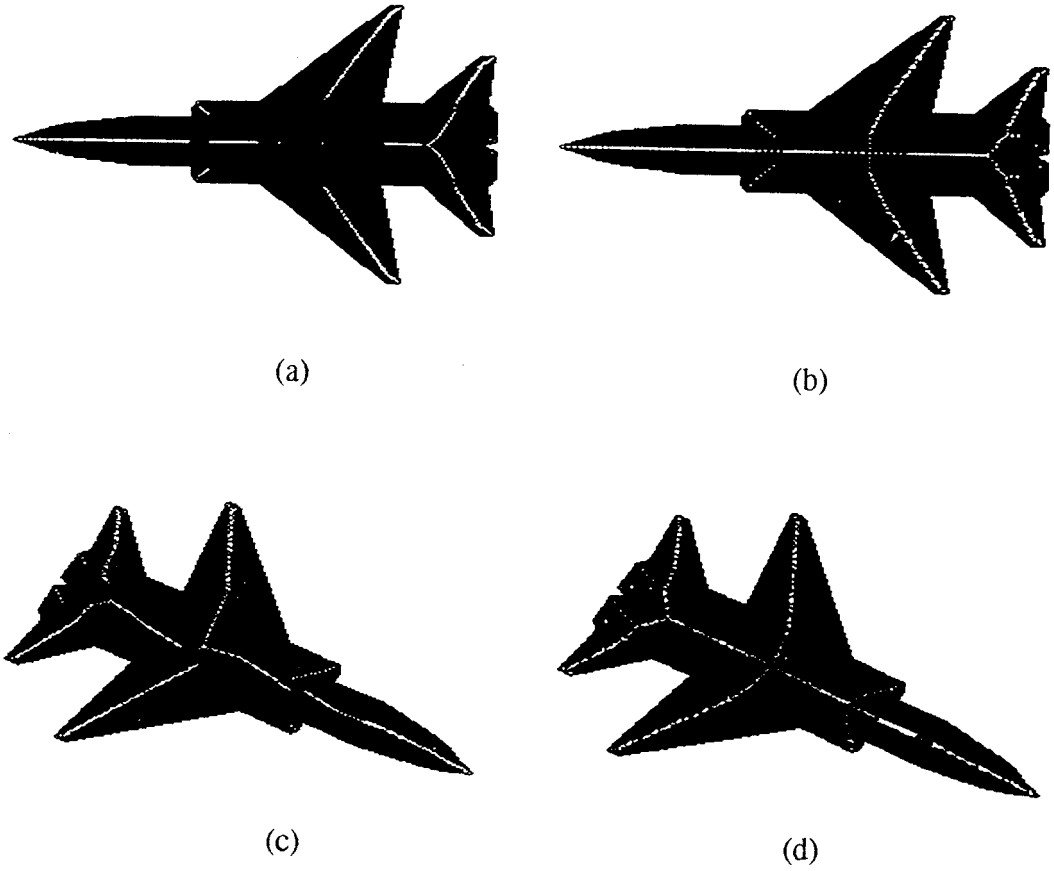

Figure 6.8.8: (a) Uniform skeleton of the object AIRPLANE; (b) Pseudo-Euclidean skeleton of the object AIRPLANE; (c) Uniform skeleton of the object AIRPLANE rotated by 210 degrees; (d) Pseudo-Euclidean skeleton of the object AIRPLANE rotated by 210 degrees.

A generalization of the concept of the skeleton to graytone images has already been suggested by various researchers [34,35,36]. As will be seen, the generalization will not be straightforward since there exist certain asymmetries between the binary and grayscale images. Let $g(x)$ be a structuring function of finite support and ng the n-fold Minkowksi addition [53]:

$$ng = g \oplus g \oplus \cdots \oplus g \tag{6.8.16}$$

The grayscale *skeleton subfunctions* $S_n(f)$ of a function f are given by:

$$S_n(f) = (f \ominus ng^s) - (f \ominus ng^s)_g \tag{6.8.17}$$

where - denotes algebraic difference. It should be noted that the definition (6.8.17) is analogous with definition (6.8.4). If g has the simple form (6.6.1), this definition is equivalent to the "min-max" approach to grayscale skeletonization [34]. Given the skeleton subfunctions $S_n(f)$, there are two ways to define the image skeleton:

$$SK_{\text{sum}}(f)(x) = \sum_{n=0}^{N} [S_n(f)](x) \qquad x \in \mathbf{Z}^n \tag{6.8.18}$$

$$SK_{\max}(f)(x) = \max_{n=0}^{N} \{[S_n(f)](x)\} \qquad x \in \mathbf{Z}^n \tag{6.8.19}$$

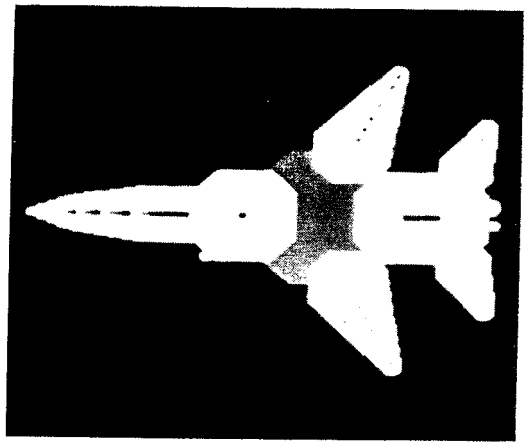

Figure 6.8.9: Partial reconstruction of the AIRPLANE by using some skeleton subfunctions.

An example of a 1-D skeleton obtained by using a 5-point structuring set $G=\{-2,-1,0,1,2\}$ is shown in Figure 6.8.10. However, the full knowledge of each skeleton subfunction $S_n(f)$, $n=1,...,N$ is required for the reconstruction of the original function:

$$f = [...[[S_N(f) \oplus g] + S_{N-1}(f)] \ominus g + \cdots] \oplus g + S_0(f) \tag{6.8.20}$$
$$\neq \sum_{n=0}^{N} [S_n(f) \oplus ng]$$

The last inequality stems from the fact that function dilation does not generally commute with function addition:

$$(f+g)\oplus h \le (f\oplus h)+(g\oplus h) \tag{6.8.21}$$

Therefore, reconstruction (6.8.20) is not analogous with the binary image reconstruction (6.8.6). Modifications of the skeleton definition so that a reconstruction scheme similar to that of (6.8.20) exists can be found in [53].

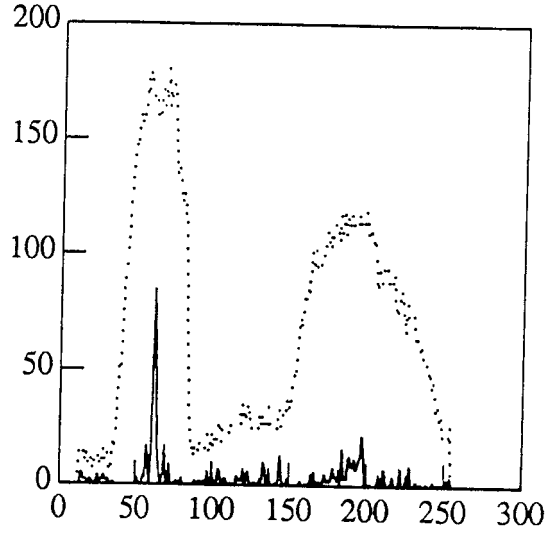

Figure 6.8.10: Skeleton $SK_{\text{sum}}(f)$ (solid curve) of an 1-D function (dotted curve).

Skeletons have already been used in several applications, e.g., in biological shape description, pattern recognition, industrial inspection, quantitative metallography, and image coding. Block-Huffman coding, run-length coding, or Elias coding schemes can be used for the coding of the skeleton subsets and Huffman code can be used for the coding of the skeleton function $skf(z)$ [24]. Compression rates up to 11:1 can be obtained by such a skeleton coding scheme. A combination of threshold decomposition and binary skeletonization has also been proposed for grayscale image coding [60].

6.9 MORPHOLOGICAL SHAPE DECOMPOSITION

Shape decomposition is a very common technique in object description [50]. It decomposes a "complex" object X into a union of "simple" subsets $X_1,...,X_n$. Such a decomposition must have the following desirable properties:

1. It should conform with our intuitive notion of simple components of a complex object.

2. It should have a well-defined mathematical characterization.
3. Its characterization must be object independent.
4. The complexity of the representation must be comparable with the complexity of the original description of X.
5. It must be invariant under translation, scaling, and rotation.
6. It should allow arbitrary amounts of detail to be computed and also allow abstraction from detail.
7. It should be fast and unique.
8. It should be stable under noise.

Usually the simple components are convex polygons [50]. However, in this case the object decomposition does not always correspond to our notion of "simple" components. Another approach to the problem could be the following. The "body" X_1 of the object X is found. This can be easily described in terms of either the maximal inscribable disk or square or rectangle or triangle in the object. The "body" X_1 is subsequently subtracted from the object X. The maximal inscribable disk or square or rectangle or triangle X_2 in the object $X - X_1$ is found. This process is repeated until all the details of the object X are described. This process can be easily described in the notation of mathematical morphology. Let B be the structuring element that represents the geometric primitive to be used in the description of X. The maximal inscribable element B in X has the form $X_1 = X_{r_1 B}$ and it has size r_1. It can be found by eroding the object X by B many times, until it vanishes. The number of erosions is the size r_1 of the maximal inscribable element B in X. This processes can be repeated for $X - X_1$. The whole procedure is called *morphological shape decomposition* and it can be described by the following recursive formula [45,46]:

$$X_i = (X - X'_{i-1})_{r_i B} \tag{6.9.1}$$

$$X'_i = \bigcup_{j=1}^{i} X_j$$

$$X'_0 = \varnothing$$

$$\textit{Stopping condition}: \quad (X - X'_K) \ominus B^s = \varnothing$$

Morphological shape decomposition decomposes an object X in a series of simple objects $X_1,...,X_n$. The object X can be reconstructed from its decomposition as follows:

$$X'_i = \bigcup_{j=1}^{K} X_j \tag{6.9.2}$$

The simple objects are of the form:

$$X_i = L_i \oplus r_i B \tag{6.9.3}$$

where L_i is either a point or a line. The objects described by (6.9.2) are the so-called *Blum ribbons* [51]. Such a Blum ribbon is shown in Figure 6.9.1. The line L is called the *spine* of the Blum ribbon.

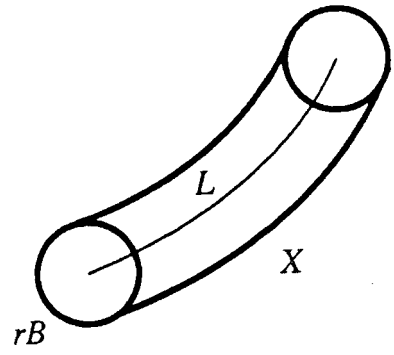

Figure 6.9.1: Example of a Blum ribbon.

Morphological shape decomposition is unique, translation and scale invariant, antiextensive, and idempotent. If the disk is used as a structuring element it is also rotation invariant. The morphological decomposition of the binary image POT, shown in Figure 6.9.2a, by using the CIRCLE and the SQUARE structuring elements is shown in Figures 6.9.2b and 6.9.2c, respectively. Morphological shape decomposition creates a tree structure for the description of an object X. The leaves of this tree are the simple components of the the object. This morphological shape decomposition tree has been successfully used for binary object recognition [48].

Usually objects can not be represented well by using one geometric primitive. The use of a multitude of structuring elements $S = \{B_1,..,B_N\}$ e.g., square, disk, triangle, gives much more descriptive power in the object representation scheme. In this case, the maximal inscribable sets $r_j B_j$, $j=1,..,N$ in the object X are found. Let $m(X)$ be a measure of the object X, e.g. the area of X. The maximal inscribable element $r_i B_i$ that minimizes $m(X - r_i B_i)$ describes the object body in the best way and it can be used as a representation of the object body. The same procedure can be repeated for the object $X - r_i B_i$. The whole procedure is described by the following recursive relation [47,55]:

$$X_i = (X - X'_{i-1})_{r_i B_i} \tag{6.9.4}$$

$$r_i B_i = \{\ B_i \in S : m(X - X'_{i-1} - r_i B_i) \qquad \textit{is minimal}\ \}$$

$$X'_i = \bigcup_{j=1}^{i} X_j$$

$$X'_0 = \varnothing$$

The morphological representation of the POT by using two structuring elements, namely the CIRCLE and the SQUARE, is shown in Figure 6.9.2d. Another morphological decomposition scheme has been proposed recently for binary shape recognition [73]. It decomposes a binary object into triangles.

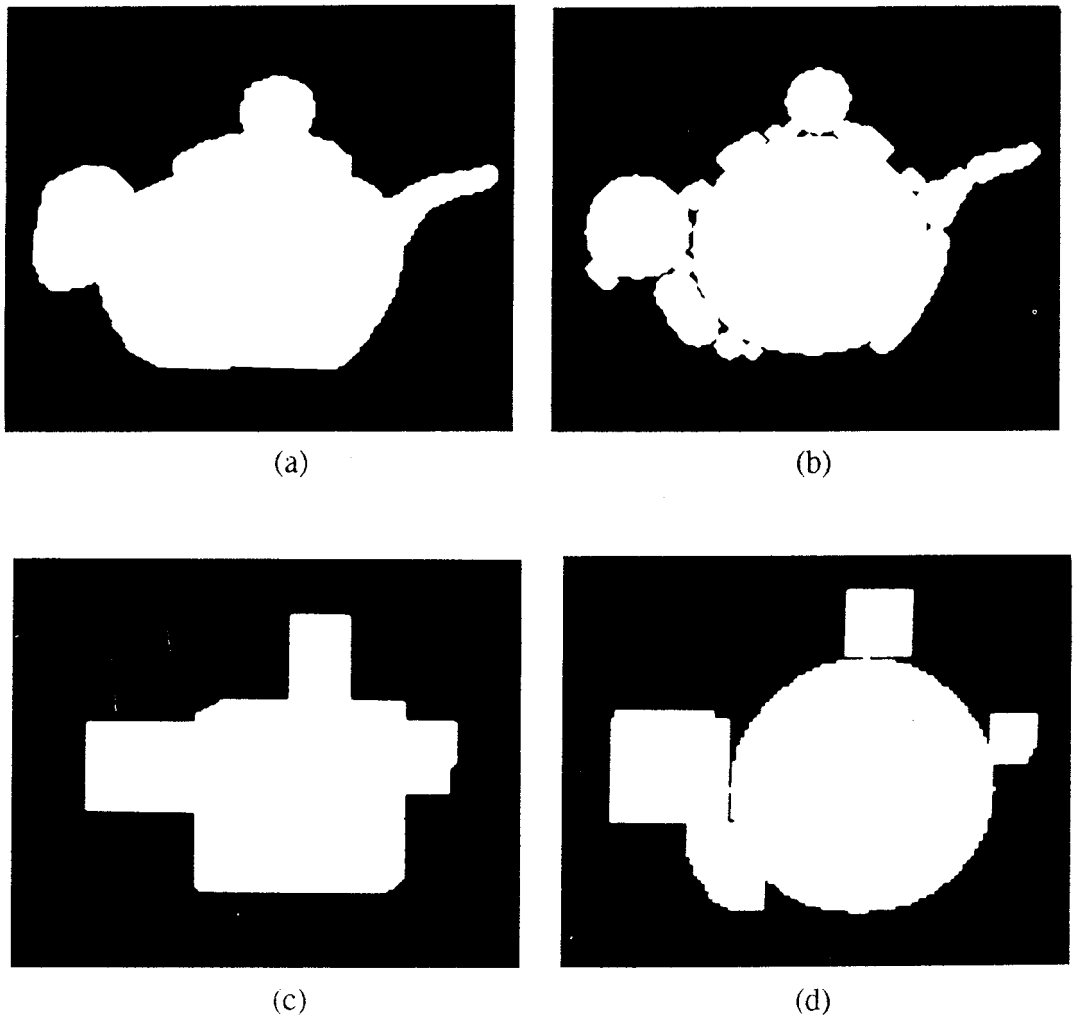

Figure 6.9.2: (a) POT; (b) Morphological decomposition of POT in a union of non-overlapping disks; (c) Morphological decomposition of POT in a union of non-overlapping squares; (d) Morphological decomposition of POT in a union of non-overlapping squares and disks.

Finally, mathematical morphology has been used for shape representation of

two-dimensional and three-dimensional objects as an extension of the Constructive Solid Geometry (CSG) which is extensively used in graphics [47,55]. A similar shape representation scheme is also proposed in [74].

The notion of decomposition can be easily extended to the morphological analysis of multivalued signal and grayscale images. In this case, a signal $f(x)$ can be decomposed in simple functions of the form:

$$f_i(x) = [l_i \oplus rg](x) \tag{6.9.5}$$

where $g(x)$ is a structuring function and $l_i(x)$ is a function having constant value $l > 0$ in its region of support L_i. A structuring function and a simple function are shown in Figures 6.9.3 and 6.9.4, respectively.

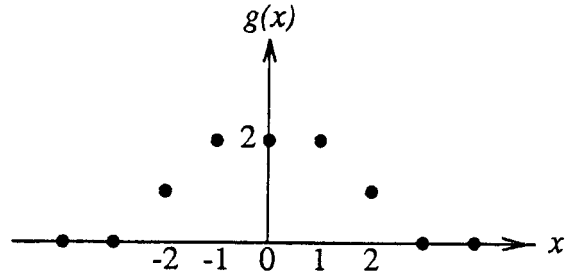

Figure 6.9.3: Structuring function.

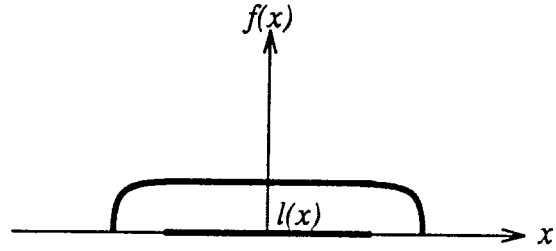

Figure 6.9.4: Simple function.

A structuring function $rg(x)$ is called maximal in the signal $f(x)$ if :

$$f(x) \ominus (r+dr)g^s(x) < 0\,, \qquad \forall x \in D \tag{6.9.6}$$

Having defined these two basic notions, the morphological analysis of $f(x)$ is given by the following recursive formula:

$$f_i(x) = (f - f'_{i-1})_{r,g}(x) \tag{6.9.7}$$

$$f'_i = \sum_{j=1}^{i} f_j(x)$$

$$f'_0(x) = 0$$

$$[(f - f'_K) \ominus g](x) < 0 \qquad \forall x \in D$$

The function $f(x)$ can be easily reconstructed from its simple components:

$$f(x) = \sum_{j=1}^{K} f_j(x) \tag{6.9.8}$$

An example of the morphological signal representation of the signal of Figure 6.9.5a is shown in Figure 6.9.5b. The structuring function used is shown in Figure 6.9.3. A partial reconstruction of this function by using only its first six simple components is shown in Figure 6.9.5b.

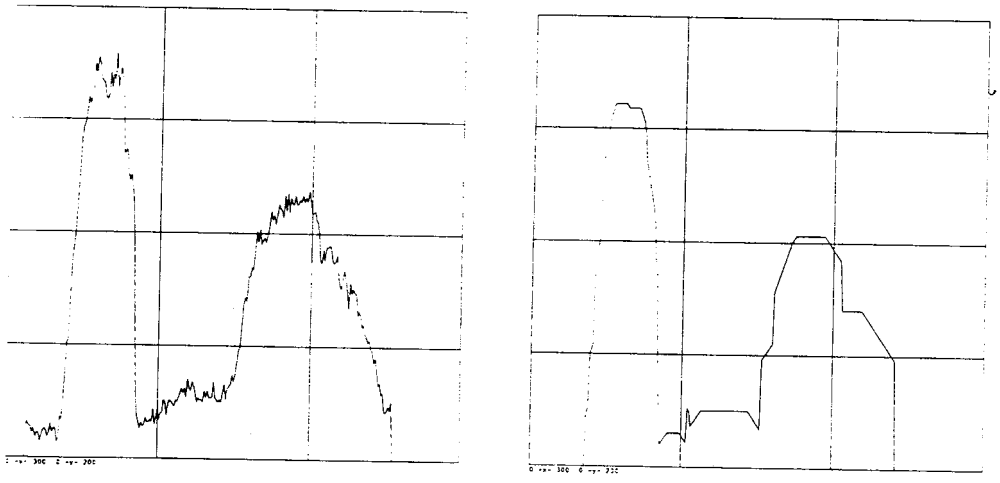

(a) (b)

Figure 6.9.5: (a) Original function; (b) Partial reconstruction of the original function by using its first six simple components.

6.10 THINNINGS AND THICKENINGS

Thinnings and thickenings are operations that are closely related to the notion of skeletonization. Their relation to the digital skeletons has been already studied in [37], [38]. Later on their relation to the morphological operations has been investigated [1, p.390],[5]. In the following a description of thinning and thickening in terms of mathematical morphology will be given. Let X be an image object and T a compact structuring element consisting of two

subsets T_1, T_2, i.e., $T=\{T_1,T_2\}$. *Thinning* $X \otimes T$ of X by T is the set subtraction:

$$X \otimes T = X - X \circledast T = X \cap [(X \ominus T_1^s) \cap (X^c \ominus T_2^s)]^c \tag{6.10.1}$$

where $X \circledast T$ is the hit-or-miss transformation (6.2.43):

$$X \circledast T = (X \ominus T_1^s) - (X \oplus T_2^s) = (X \ominus T_1^s) \cap (X^c \ominus T_2^s) \tag{6.10.2}$$

Its dual operation is *thickening*:

$$X \odot T = X \cup (X \circledast T) \tag{6.10.3}$$

Thinning and thickening are dual to each other by complementation:

$$(X \odot T)^c = X^c \otimes T^* \tag{6.10.4}$$

where

$$T^* = \{T_2, T_1\}.$$

Definitions (6.10.1-2) have a meaning if the subsets T_1, T_2 do not intersect each other, i.e., if $T_1 \cap T_2 = \varnothing$. If they intersect each other, both thinning and thickening are equivalent to X:

$$T_1 \cap T_2 \neq \varnothing \Rightarrow X \otimes T = X \odot T = X \tag{6.10.5}$$

If T_2 contains the origin, the thinning $X \otimes T$ coincides to X. If T_1 contains the origin, the thickening $X \odot T$ coincides with X:

$$\{0\} \in T_2 \Rightarrow X \otimes T = X \quad \text{for every } T_1 \tag{6.10.6}$$

$$\{0\} \in T_1 \Rightarrow X \odot T = X \quad \text{for every } T_2 \tag{6.10.7}$$

The two parts of the structuring element T are chosen to be disjoint and not to contain the origin (in T_1 for thickening and in T_2 for thinning) in order to avoid trivial results. By definition, the thickenings are extensive and the thinning antiextensive:

$$T' \subset T \Rightarrow X \otimes T' \subset X \otimes T \subset X \subset X \odot T \subset X \odot T' \tag{6.10.8}$$

where the set inclusion $T' \subset T$ means also subset inclusion: $T_1' \subset T_1$ and $T_2' \subset T_2$.

Thinnings and thickenings are translation and scale invariant since their definitions (6.10.1), (6.10.2) employ erosion which is translation and scale invariant. Furthermore the operations in their definition require only local knowledge of object X since they are local operations. The semicontinuity of erosion implies that, for a closed set X and compact structuring elements T, the thinning $X \otimes T$ is an upper semicontinuous transformation [1]. The thickening $X \odot T$ is a lower semicontinuous transformation if X is an open set. Therefore, thinning and thickening are morphological transformations.

An extension of thinning is the *sequential thinning*. Let $T_i=\{T_{1i},T_{2i}\}$ be a sequence of structuring elements. The sequential thinning is defined as [5]:

$$...(...((X \circ T_1) \circ T_2) \cdots \circ T_i) \cdots = X \circ \{T_i\} \tag{6.10.9}$$

It can be proven that if T_i is infinite, $X \circ \{T_i\}$ is idempotent. If T_{i+1} is derived from T_i by a rotation of 60 degrees, the corresponding sequence is called *standard* and the sequential thinning (6.10.9) is denoted by $X \circ \{T\}$.

6.11 GRANULOMETRIES AND THE PECSTRUM

The fundamental approach of morphological image analysis is to transform an image object X by a morphological transformation ψ and then to measure the transformed image:

$$X \rightarrow \psi(X) \rightarrow m(\psi(X)) \tag{6.11.1}$$

This approach is clearly illustrated in Figure 6.1.1. One of the most basic measures of the transformed image $\psi(X)$ is the area of $\psi(X)$. Usually a family of transformations $\psi_r(X)$ is used, where r is a parameter. Such a family consists of the openings X_{rB} of object X with a structuring element rB of size r. The mapping

$$r \in \mathbf{R} \rightarrow X_{rB} \tag{6.11.2}$$

is called *granulometry*. Matheron [3] has introduced a general theory of granulometries, with axiomatic basis, whose special case is the opening (6.11.2). However, the present discussion will be limited to (6.11.2) because it is very interesting from a practical point of view. A consequence of (6.11.2) is that there exists a real-valued function $u(r)$ that gives the measure of X_{rB}:

$$r \in \mathbf{R} \rightarrow u(r) = m(X_{rB}) \in \mathbf{R} \tag{6.11.3}$$

This function is called *size distribution* of X_{rB}. From a physical point of view, the size distribution of X gives the area of X which can be covered by a disk rB of radius r, when this disk moves *inside* the object X. The greater the radius is, the smaller the area. Therefore, the size distribution $u(r)$ is a strictly monotone function. Furthermore, $u(r)$ depends greatly on the shape of the structuring element B. However, the interest lies in the fact that different objects X give different size distributions, when opened by the same structuring element B. Therefore, granulometries can be used for pattern recognition, as will be seen later on. From another point of view, granulometric processes can be considered as a type of filtering that removes the sections of the image object X, which are not sufficiently large to include the structuring element rB. Such an interpretation of granulometries is shown in Figure 6.11.1. Therefore, a granulometry can be thought as a one-parameter family of low-pass filters.

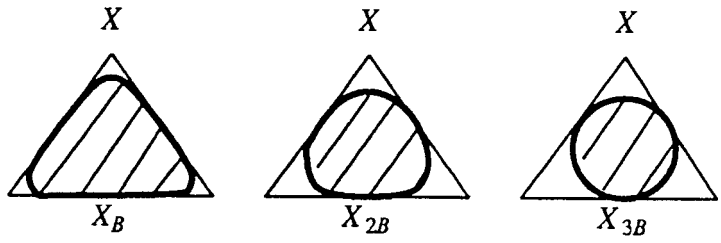

Figure 6.11.1: Opening of a set X by disks of increasing size.

Granulometries $\psi_r(X)$ possess several useful algebraic properties. Some of them will be repeated here without proof, when $\psi_r(X)=X_{rB}$ [9, pp. 120, 163]:

(1) $\psi_r(X)\subset X$ for any $r>0$.

(2) $r\geq s$ implies that $\psi_r(X)\subset\psi_s(X)$.

(3) $A \subset X$ implies that $\psi_r(A)\subset\psi_r(X)$.

This property simply states that the granulometry X_{rB} is increasing transformation.

(4) $$\psi_r[\psi_s(X)] = \psi_s[\psi_r(X)] = \psi_{\max(r,s)}(X) \tag{6.11.4}$$

This operation states that opening by an iteration of sB and rB is equivalent to opening by tB, where t is the maximum of r,s. The properties (2)-(4) are the axioms that must be satisfied by every granulometry.

(5) Granulometry X_{rB} is translation and scale invariant:

$$\psi_r(X_z) = [\psi_r(X)]_z \tag{6.11.5}$$

$$\psi_r(X) = \lambda\psi_r(\frac{1}{\lambda}X) \tag{6.11.6}$$

Granulometries satisfying (6.11.5-6) are called *Euclidean granulometries.*

The size distribution $u(r)$ is a strictly monotonically decreasing function. Therefore, its normalized negative derivative $f(r)$ can be used instead:

$$f(r) = \frac{-\frac{d}{dr}[m(\psi_r(X))]}{m(X)} \tag{6.11.7}$$

The division by the area $m(X)$ of X is a simple scaling, because $m(X)$ does not depend on r. Function $f(r)$ is called *pattern spectrum* or *pecstrum* [39,40,53,54,56,81]. An example of the pecstrum is shown in Figure 6.11.2. The structuring element B used in this example was a square of unit dimensions. The object shown in Figure 6.11.2a has simple shape. Its pecstrum is a delta function as can be seen in Figure 6.11.2c. The object shown in Figure 6.11.2d has a more

complex shape. Its pecstrum has another delta function at a smaller value of r, as can be seen in Figure 6.11.2f. This component of the pecstrum is due to the "jagginess" of the object contour.

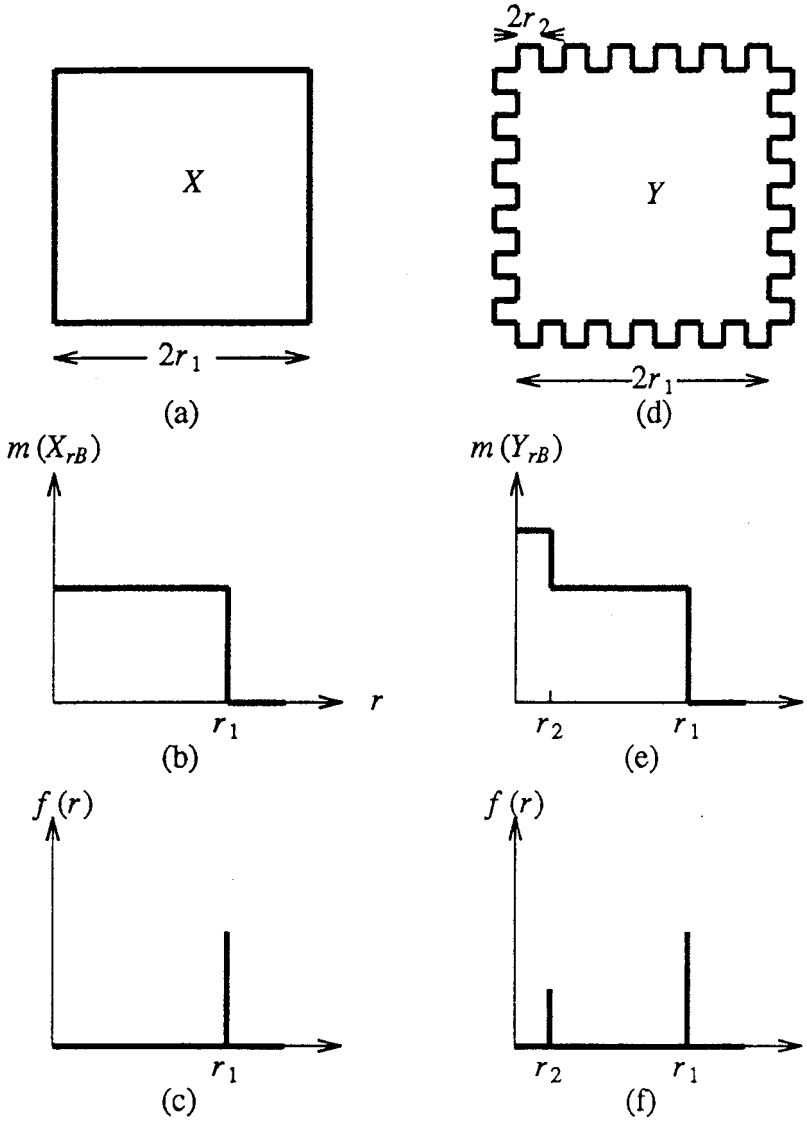

Figure 6.11.2: (a) Object X; (b) Function $m(X_{rB})$; (c) Pecstrum $f(r)$ of X; (d) Object Y; (e) Function $m(Y_{rB})$; (f) Pecstrum $f(r)$ of Y.

A digital version of the pecstrum is the following:

$$f(n) = \frac{m(\psi_n(X)) - m(\psi_{n+1}(X))}{m(X)} = \frac{m(X_{nB}) - m(X_{(n+1)B})}{m(X)} \qquad (6.11.8)$$

There exist two conceptual similarities between frequency spectrum and pecstrum:

(1) The spectrum is obtained by transforming the signal through a multiplication by a complex exponential $e^{i\omega x}$ of a certain frequency ω, whereas the pecstrum is obtained by transforming the signal by taking its opening with respect to a certain structuring element.

(2) The magnitude of the frequency spectrum of a signal at a frequency ω is the *spectral content* of the signal in this frequency, whereas the pecstrum gives the pattern content of the signal.

The area under the pecstrum is one:

$$\int_0^\infty f(r)dr = 1 \tag{6.11.9}$$

This property can be easily proved by using the definition (6.11.7). It can also be proven by using Proposition 6.8.9 and (6.11.8) that if an object X has the k minimal skeleton subsets empty, its first k size pecstrum samples are zero [56]. Rotation and size invariant modifications of the pecstrum are described in [61].

Pecstra can be used for pattern recognition [40]. If $f_R(n)$ is a reference pecstrum and $f(n)$ is the pecstrum of a new object X, the distance d:

$$d = \left[\sum_{n=0}^{N-1} c_n(f(n)-f_R(n))^2\right]^{1/2} \tag{6.11.10}$$

can be used to decide if the new object coincides with a reference pattern.

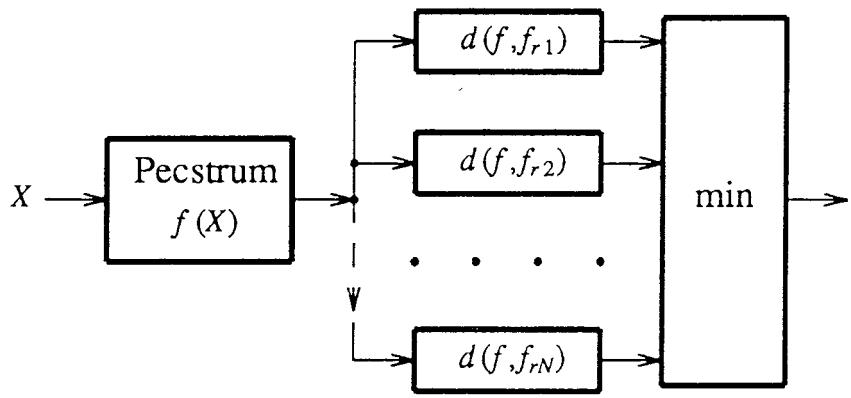

Figure 6.11.3: Pattern recognition scheme using comparisons of the pecstrum of an object with reference pecstra.

Such a pattern recognition scheme is shown in Figure 6.11.3. The weights c_n can be chosen to be equal to unity, if no specific parts of pecstrum differences are emphasized. The weights c_n can also be used to emphasize certain parts of the object pecstrum. If the large differences from the reference pecstrum are to be emphasized, the weights can be chosen as follows:

$$c_n = exp\,(a\,[f\,(n)-f_R(n)]^2)\,, \qquad a>0 \tag{6.11.11}$$

or

$$c_n = exp\,(a\,|f\,(n)-f_R(n)|\,)\,, \qquad a>0 \tag{6.11.12}$$

The choice of the appropriate value of the parameter a is usually application dependent.

6.12 DISCUSSION

Mathematical morphology comes from a completely different mathematical background than the rest of the digital signal and image processing techniques. Thus it has found many applications in the cases where the description of geometrical and topological information about images or objects is important. Such cases usually are found in image analysis applications. However, it has been proven that mathematical morphology techniques can also be applied in digital image processing. The use of mathematical morphology in image processing has been greatly enhanced by extending the notions of morphology from binary images to multivalued signals and images (grayscale morphology). Another reason for the recent popularity of mathematical morphology is that it employs simple mathematical operations which can be programmed easily and computed very fast on any computer. Furthermore, the morphological operations can be easily implemented in parallel or pipelined architectures, thus tremendously increasing the speed of their execution. Such architectures are described in a subsequent chapter.

Mathematical morphology is one of the most active research areas in nonlinear image processing. This chapter covers most of the basic theory of mathematical morphology as well as several recent research results. The interested reader can find more theoretical results in a recent book edited by Serra [6] and in a special issue on mathematical morphology in *Signal Processing* [75-80]. More information on the skeleton properties can be found in [6], [77]. Extensions of mathematical morphology to general image algebras can be found in [68]. Its use in L_1 norm image matching and correlation is described in [62]. Its application in the texture analysis of seismic images, in the computation of non-planar point neighborhoods on cellular automata and in the 3-d scene segmentation can be found in [69, 70, 71], respectively. The processing

of graphs by mathematical morphology tools is addressed in [78]. Finally, speckle noise removal and image modelling by mathematical morphology are described in [76, 80], respectively.

REFERENCES

[1] J. Serra, *Image analysis and mathematical morphology*, Academic Press, 1983.

[2] James and James, *Mathematical dictionary*, Van Nostrand, 1976.

[3] G. Matheron, *Random sets and integral geometry*, J. Wiley, 1975.

[4] R.M. Haralick, S.R. Sternberg, X. Zhuang, "Image analysis using mathematical morphology", *IEEE Transactions on Pattern Analysis and Machine Intelligence*, vol. PAMI-9, no. 4, pp. 532-550, July 1987.

[5] J. Serra, "Introduction to mathematical morphology", *Computer Vision, Graphics and Image Processing*, vol. 35, pp. 283-305, 1986.

[6] J. Serra (editor), *Image analysis and mathematical morphology: theoretical advances*, vol. 2, Academic Press, 1988.

[7] H. Minkowski, "Volumen und oberflaechen", *Math. Annalen*, vol. 57, pp. 447-495, 1903.

[8] C.R. Giardina, E.R. Dougherty, *Morphological methods in image and signal processing*, Prentice Hall, 1988.

[9] E.R. Dougherty, C.R. Giardina, *Image processing - continuous to discrete*, vol. 1, Prentice-Hall, 1987.

[10] V. Goetcherian, "From binary to gray level tone image processing using fuzzy logic concepts", *Pattern Recognition*, vol. 12, pp. 7-15, 1980.

[11] C. Lantuejoul, J. Serra, "M-filters", *Proc. IEEE Int. Conf. on ASSP*, pp. 2063-2066, 1982.

[12] F. Meyer, "Contrast feature extraction", in *Quantitative Analysis of Microstructures in Material Sciences, Biology and Medicine*, Special issue of Practical Metallography, J.L. Charmont editor, Reidner-Verlag, 1977.

[13] A. Rosenfeld, "Connectivity in digital pictures", *J. Assoc. Comput. Mach.*, vol. 17, no. 1, pp. 146-160, 1970.

[14] S.R. Sternberg, "Parallel architecture for image processing", *Proc. 3rd COMPSAC*, Chicago, 1979.

[15] J. Serra, *Morphologie pour les fonctions "a peu pres en tout ou rien"*, Tech. report Centre de Morphologie Mathematique, Fontainebleau, France, 1975.

[16] C. Lantuejoul, *Sur le modele de Johnson-Mehl generalise*, Tech. report Centre de Morphologie Mathematique, Fontainebleau, France, 1977.

[17] S.R. Sternberg, "Biological image processing", *Computer*, pp. 22-34, Jan. 1983.

[18] S.R. Sternberg, "Grayscale morphology", *Computer Vision, Graphics and Image Processing*, vol. 35, pp. 333-355, 1986.

[19] R.L. Stevenson, G.R. Arce, "Morphological filters: statistics and further syntactic properties", *IEEE Transactions on Circuits and Systems*, vol. CAS-34, pp.1292-1305, Nov. 1987.

[20] F. Meyer, "Iterative image transformations for an automatic screening of cervical smears", *J. Histoch. Cytochem.*, vol. 27, pp. 128-135, 1979.

[21] F. Meyer, "Automatic screening of cytological specimens", *Computer Vision, Graphics and Image Processing*, vol. 35, pp. 356-369, 1986.

[22] S.D. Pass, "Segmentation by shape discrimination using spatial filtering techniques", in *Digital Image Processing*, J.C. Simon and R.M. Haralick editors, D. Reidel Publ. Co., 1981.

[23] H.P. Kramer, J.B. Bruckner, "Iterations of nonlinear transformation for enhancement of digital images", *Pattern Recognition*, vol. 7, 1975, pp. 53-58.

[24] P.Maragos, R.W. Schafer, "Morphological skeleton representation and coding of binary images", *IEEE Transactions on Acoustics, Speech and Signal Processing*, vol. ASSP-34, no.5, pp. 1228-1244, Oct. 1986.

[25] H. Blum, "A transformation for extracting new descriptors of shape", *Models for the Perception of Speech and Visual Forms*, W. Wathen-Dunn editor, pp. 362-380, MIT Press, 1967.

[26] H. Blum, "Biological shape and visual sciences (part I)", *J. Theoret. Biology*, vol. 38, pp. 205-287, 1973.

[27] J.C. Kotelly, "A mathematical model of Blum's theory of pattern recognition", Rep. 63-164, Airforce Cambridge Res. Labs, Mass., 1963.

[28] L. Calabi, "A study of the skeleton of plane figures", Res. SR20-60429, Parke Mathematical Labs., Mass., 1965.

[29] A. Rosenfeld, J.L. Pfalz, "Sequential operations in digital picture processing", *J. Assoc. Comput. Mach.*, vol. 13, pp. 471-494, Oct. 1966.

[30] J.C. Mott-Smith, "Medial axis transformations", in *Picture Processing and Psychopictorics*, B.S. Lipkin and A. Rosenfeld editors, Academic,

1970.

[31] U. Montanari, "A method for obtaining skeletons using a quasi-Euclidean distance", *J. Assoc. Comput. Mach.*, vol. 15, pp. 600-624, Oct. 1968.

[32] C. Lantuejoul, *La squelettisation et son application aux mesures topologiques des mosaiques polycristallines*, These de Docteur-Ingenieur, Ecole de Mines, Paris, 1978.

[33] C. Lantuejoul, "Skeletonization in quantitative metallography", in *Issues of Digital Image Processing*, R.M. Haralick and J.C. Simon editors, Sitjhoff and Noordhoff, 1980.

[34] S. Peleg, A. Rosenfeld, "A min-max medial axis transformation", *IEEE Trans. on Pat. Anal. Machine Intelligence*, vol. PAMI-4, no. 4, pp. 419-421, July 1982.

[35] N. Ahuja, L.S. Daris, D.L. Milgram, A. Rosenfeld, "Piecewise approximation of pictures using maximal neighborhoods", *IEEE Trans. Comput.*, vol. C-27, pp. 375-379, 1978.

[36] S. Lobregt, P.W. Verbeek, F.C.A. Groen, "Three dimensional skeletonization: principles and algorithms", *IEEE Transactions on Pattern Analysis and Machine Intelligence*, vol. PAMI-2, no.1, pp.75-77, Jan. 1980.

[37] A. Rosenfeld, A.C. Kak, *Digital picture processing*, Academic Press, 1976.

[38] S. Levialdi, "Parallel pattern processing", *IEEE Trans. System, Man and Cybern.*, SMC-1, pp. 292-296, 1971.

[39] J.F. Bronskill, A.N. Venetsanopoulos, "The pecstrum", *3rd ASSP Workshop on Spectral Estimation and Modelling*, Boston, 1986.

[40] J.F. Bronskill, A.N. Venetsanopoulos, "Multidimensional shape recognition using mathematical morphology", *Proc. Int. Workshop on Time-Varying Image Processing and Moving Object Recognition*, Florence, Italy, pp. 3-18, 1986.

[41] P.Maragos, R.W. Schafer, "Morphological filters, part I: their set theoretic analysis and relations to linear shift invariant filters", *IEEE Transactions on Acoustics, Speech and Signal Processing*, vol. ASSP-35, no.8, pp. 1153-1169, Aug. 1987.

[42] P.Maragos, R.W. Schafer, "Morphological filters, part II: their relations to median, order statistic and stack filters", *IEEE Transactions on Acoustics, Speech and Signal Processing*, vol. ASSP-35, no.8, pp. 1170-1184, Aug. 1987.

[43] Z. Zhou, A.N. Venetsanopoulos, "Analysis and implementation of morphological skeleton transforms", *IEEE Transactions on Acoustics, Speech and Signal Processing*, in press.

[44] Z. Zhou, A.N. Venetsanopoulos, "Morphological skeleton representation and shape recognition", *Proc. IEEE Int. Conf. on Acoustics, Speech and Signal Processing*, pp. 948-951, New York, 1988.

[45] I. Pitas, A.N. Venetsanopoulos, "Morphological shape decomposition", *IEEE Transactions on Pattern Analysis and Machine Intelligence*, in press, Jan. 1990.

[46] I. Pitas, A.N. Venetsanopoulos, "Morphological shape decomposition", *Proc. IEEE Int. Conf. on Computer Vision*, London, 1987.

[47] I. Pitas, A.N. Venetsanopoulos, "Morphological shape representation", *Computer Vision, Graphics and Image Processing*, under review.

[48] I. Pitas, N. Sidiropoulos, "Pattern recognition of binary image objects by using morphological shape decomposition", *Computer Vision, Graphics and Image Processing*, under review.

[49] I. Pitas, "Morphological signal analysis", *IEEE Transactions on Acoustics, Speech and Signal Processing*, under review.

[50] T. Pavlidis, "A review of algorithms for shape analysis", *Computer Graphics and Image Processing*, vol. 7, no.2, pp. 243-258, April 1978.

[51] A. Rosenfeld, "Axial representations of shape", *Computer Vision, Graphics and Image Processing*, vol. 33, pp. 156-173, 1986.

[52] Z. Zhou, A.N. Venetsanopoulos, "Pseudo-euclidean morphological skeleton transform for machine vision", *Proc. 1989 IEEE Int. Conf. on Acoustics, Speech and Signal Processing*, Glasgow, England, 1989.

[53] P. Maragos, *A unified theory of translation invariant systems with applications to morphological analysis and coding of images*, Ph.D. Thesis, Georgia Institute of Technology, 1985.

[54] J.F. Bronskill, A.N. Venetsanopoulos, "Multidimensional shape description and recognition using mathematical morphology", *Journal of Intelligent and Robotic Systems*, vol. 1, pp. 117-143, 1988.

[55] I. Pitas, A.N. Venetsanopoulos, "Morphological shape representation and recognition", *Proc. 3rd Workshop on Time-varying Image Processing and Object Recognition*, Florence, Italy, 1989.

[56] P. Maragos, "Pattern spectrum of images and morphological shape-size complexity", *Proc. 1987 IEEE Int. Conf. on Acoustics, Speech and Signal Processing*, pp. 241-244, Dallas, USA, 1987.

[57] K. Preston Jr., "Ξ filters", *IEEE Transactions on Acoustics, Speech and Signal Processing*, vol. ASSP-31, pp.861-876, Aug. 1983.

[58] F.Y.C. Shih, O.R. Mitchell, "Threshold decomposition of grayscale morphology into binary morphology", *IEEE Trans. on Pat. Anal. Machine*

Intelligence, vol. PAMI-11, no. 1, pp. 31-42, Jan. 1989.

[59] X. Zhuang, R.M. Haralick, "Morphological structuring element decomposition", *Computer Vision, Graphics and Image Processing*, vol.35, pp. 370-382, 1986.

[60] S.A. Rajala, H.A. Peterson, E.L. Delp, "Binary morphological coding of grayscale images", *Proc. IEEE Int. Symp. on Circuits and Systems*, pp. 2807-2811, Helsinki, Finland, 1988.

[61] M. Binaghi, V. Cappellini, C. Raspolini, "Description and recognition of multidimensional signals using rotation and scale invariant morphological transformations", *Proc. European Signal Processing Conference*, 1988.

[62] P. Maragos, "Optimal morphological approaches to image matching and object detection", *Proc. IEEE Int. Conf. on Computer Vision*, pp. 695-699, Tampa, Florida, 1988.

[63] J.S.J Lee, R.M. Haralick, L.G. Shapiro, "Morphological edge detection", *International Journal of Robotics and Automation*, vol. RA-3, no. 2, pp. 142-156, 1987.

[64] R.J. Feehs, G.R. Arce, "Multidimensional morphological edge detection", *SPIE Visual Computing and Image Processing II*, pp.285-292, 1987.

[65] J.A. Noble, "Morphological feature detection", *Proc. IEEE Int. Conf. on Computer Vision*, pp. 112-115, Tampa, Florida, 1988.

[66] W. Kohler, *Gestalt psychology*, Liveright Pub. Co., 1970.

[67] R.M. Haralick, X. Zhuang, C. Lin, J. Lee, "The digital morphological sampling theorem", *Proc. IEEE Int. Symp. on Circuits and Systems*, pp. 2789-2791, Helsinki, Finland, 1988.

[68] G.X. Ritter, J.L. Davidson, J.N. Wilson, "Beyond mathematical morphology", *SPIE Visual Computing and Image Processing II*, vol. 845, pp.260-268, 1987.

[69] K. Kotropoulos, I. Pitas, "Texture analysis and segmentation of seismic images", *Proc. 1989 IEEE Int. Conf. on Acoustics, Speech and Signal Processing*, pp. 1437-1440, Glasgow, England, 1989.

[70] M.M. Skolnik, S. Kim, R. O'Bara, "Morphological algorithms for computing nonplanar point neighborhoods on cellular automata", *Proc. IEEE Int. Conf. on Computer Vision*, pp. 106-111, Tampa, Florida, 1988.

[71] C.D. Brown, R.W. Marvel, G.R. Arce, C.S. Ih, D.A. Fertell, "Morphological 3-d segmentation using laser structured light", *Proc. IEEE Int. Symp. on Circuits and Systems*, pp. 2803-2805, Helsinki, Finland, 1988.

[72] C.-H. H. Chu, E.J. Delp, "Impulsive noise suppression and background normalization using morphological operators", *IEEE Transactions on Biomedical Engineering*, vol. BME-36, no. 2, pp. 262-273, Feb. 1989.

[73] Y. Zhao, R.M. Haralick, "Binary shape recognition based on automatic morphological shape decomposition", *Proc. IEEE International Conference on Acoustics, Speech and Signal Processing*, pp. 1691-1694, Glasgow, Scotland, 1989.

[74] P.K. Ghosh, "A mathematical model for shape description using Minkowski operators", *Computer Vision Graphics and Image Processing*, vol. 43, no. 3, pp. 239-269, Dec. 1988.

[75] F. Meyer, J. Serra, "Contrasts and activity lattice", *Signal Processing*, vol. 16, no. 4, pp. 303-317, April 1989.

[76] F. Safa, G. Flouzat, "Speckle removal on radar imagery based on mathematical morphology", *Signal Processing*, vol. 16, no. 4, pp. 319-333, April 1989.

[77] F. Meyer, "Skeletons and perceptual graphs", *Signal Processing*, vol. 16, no. 4, pp. 335-363, April 1989.

[78] L. Vincent, "Graphs and mathematical morphology", *Signal Processing*, vol. 16, no. 4, pp. 365-388, April 1989.

[79] M. Schmitt, "Mathematical morphology and artificial intelligence: an automatic programming system", *Signal Processing*, vol. 16, no. 4, pp. 389-401, April 1989.

[80] D. Jeulin, "Morphological modelling of images by sequential random functions" *Signal Processing*, vol. 16, no. 4, pp. 403-431, April 1989.

[81] P. Maragos, "Pattern spectrum and multiscale shape representation", *IEEE Transactions on Pattern analysis and Machine Intelligence*, vol. PAMI-11, no. 7, pp. 701-716, July 1989.